Modelling of the thermal history of the Carboniferous Lorraine Coal Basin: Consequences for coal bed methane

A. Izart, J. Barbarand, R. Michel, V.A. Privalov

Modelling of paleotemperatures and hydrocarbon generation and storage in the Carboniferous Lorraine coal Basin

A.Izart [a*], J. Barbarand [b], R. Michels [a], V.A. Pryvalov [a]

[a] *UMR 7566 CNRS, Georessources, Université de Lorraine, BP23, F-54501 Vandoeuvre-les-Nancy, France*

[b] *UMR 8148 CNRS, IDES, Université de Paris-Sud 11, Bâtiment 504, F-91405 Orsay, France*

* Corresponding author: Tel: +33 9 50 96 78 75, *E-mail address:* izart.alain@voila.fr (A.Izart)

Abstract

This paper proposes a new scenario for the thermal history of the Carboniferous Lorraine coal Basin following a new tectonic model developed by Averbuch et al. (2012) and addresses some consequences for the petroleum system and CBM exploitation. Fifteen boreholes have been sampled for organic matter maturation data (Vitrinite Reflectance) and five seismic lines acquired in the eastern Lorraine have been used to characterize the Lorraine coal Basin evolution. Mesozoic and Paleozoic overburials have been calculated using Petromod software. Results show that (1) Paleozoic erosion may be estimated at a maximum of 1200m which represents a low amplitude event ; (2) little erosion occurred between Upper Paleozoic and Lower Mesozoic : paleotemperature offset is about 20°C (respectively 0,7 and 0,5 for VR data) ; (3) Cretaceous cover has a maximum thickness of 300m and decreases eastwards ; and (4) the variable HF agree well with the compressive and extensive phases of Paleozoic and extensive phase of Mesozoic. Consequences on the petroleum system are the following : (1) the organic matter of sedimentary rocks is immature in the Jurassic and Triassic rocks, mature (oil window) in the Permian, Stephanian and Westphalian D, highly mature (gas window) in Westphalian B-C and overmature in Namurian-Westphalian A ; (2) the oil and gas generation masses (Mtons/km3 of rock) are respectively for the Westphalian A, B and C equal to 0.5-8 and 0.5-20 in the EPLY 02-LOR 09 and TOUL 08 seismic lines ; (3) the oil and gas storage masses (Mtons/km3 of rock) for the Westphalian A, B and C are respectively equal to 0-0.5 and 0-0.25 except 50 in some traps along faults in anticlines in the EPLY 02-LOR 09 seismic lines and except 1 in some traps in eastern anticline in the TOUL 08 seismic line ; (4) the oil and gas of the Carboniferous rocks in Lorraine migrate upward along faults and across sediments from syncline to anticline to the Westphalian top, Stephanian, Buntsandstein and Muschelkalk or escapes laterally towards the East. The Keuper halite constitutes a barrier for the migration ; (5) as the expulsion onset began in Permian, a great part of generated oil and gas during the Carboniferous was lost. Some traps formed by small horst capped by impermeable claystone stored the oil in Forcelles and gas in Trois-Fontaines in the Muschelkalk dolomite or sandstone. The Lorraine coal basin is therefore a target for coal gas, which explains the drillings for coal gas from 1960 to now in Lorraine by numerous oil and

gas companies. The methane adsorption capacity of coal and the presence of a natural cleat system inside coal will allow a good CBM exploitation in this basin.

Keywords : Paris Basin, Lorraine coal Basin, Carboniferous, Thermal modelling, Oil and Gas.

1) Introduction

There are some papers on the paleothermicity and coal gas modelling of the Carboniferous basins in diverse tectonic contexts. Littke (2000) and Hertle and Littke (2000) modelled the paleotemperatures in the Ruhr and Saar coal basins in Germany respectively located in a foreland basin from the Rhenohercynian zone and a synorogenic basin developed on top of the Saxothuringian retro-wedge with the Petromod software. Alsaab et al. (2008) modelled the paleotemperatures and gas generation and storage in the Donbas fold belt (Ukraine) in a rift context folded during the Permian and Cretaceous with the Petromod software. Milton-Worssell et al. (2010) described Carboniferous petroleum system beneath the Central North Sea in a rift context. Faure et al. (2004) modelled the Alberta foothills and adjacent foreland, West of Calgary (Canada) in a compression context and Paleozoic and Mesozoic source rocks with the IFP softwares.

The aim of our paper is to propose a modelling with Petromod software to reconstruct the paleotemperatures and hydrocarbons generation and storage in the Lorraine Basin (France) that is in the extension of the Saar Basin in Germany and presents the same tectonic context during the Carboniferous, but with a mesozoic cover. The feasibility of CBM exploitation in this basin was checked by the data on adsorption capacity of coals and cleat system in coals.

2) Geological introduction

2.1) Geological setting

A geological map of the Mesozoic cover from Lorraine is presented in Fig. 1a. A geological map of Lorraine at Paleozoic top (Fig. 1b) locates the boreholes used in this paper (Table 1), and the Carboniferous and Permian basins under the Mesozoic cover. The Fig.1c shows the location of this Carboniferous basin in the Variscan chain.

Sedimentary infilling of the Lorraine area has been built in two periods : Late Paleozoic when Lorraine represented a limnic coal basin in the frame of the Variscan chain and Lower Mesozoic when Lorraine was part of the newly-born Paris Basin. The present-day sedimentary cover is reported in Figure 2 and characterized this succession. The Lorraine coal Basin (Fig. 2) contains a thick series (8000m) of sandstones, coals and claystones deposited from Mississipian: Late Viséan and Namurian (Serpukhovian) to Pennsylvanian : Westphalian and Stephanian. After Donsimoni (1981), the sedimentation began after the Sudete phase (Namurian) in the Lorraine coal Basin during a period of distension. Folds and the South Fault resulted of the Saalian compressive phase between the Autunian and the Saxonian. Normal faults in distension occured during the Saxonian and the Mesozoic. The Namurian and Westphalian Basin was located in the outer Saxo-Thuringian zone or Mid-German crystalline zone between the Hunsruck-Taunus Fault at West and the inner Saxo-Thuringian zone at East (Fig. 1c). However a new tectonic sketch of the Lorraine coal Basin

was proposed by Averbuch et al. (2012) with a compression during Westphalian D (Asturian phase). Three erosion phases (Fig. 2) are recognized during the Paleozoic at the Stephanian base, Late Permian base and Triassic base (Donsimoni, 1981). After the variscan orogeny and the following peneplaination, the area was an area of continental (Buntsandstein sandstone), then marine (Muschelkalk limestone) and finally lagoonal (Keuper salt) sedimentation during Triassic (Bourquin and Guillocheau, 1996 ; Bourquin et al., 2002, 2006 and 2009 ; Duringer and Vecsei, 1998) followed by a marine realm during Jurassic and Cretaceous (Guillocheau et al., 2000 ; Durlet and Thierry, 2000). The area was part of thre Paris Basin, a large intracontinental basin developed after a aborted Permian rifting (Megnien, 1980 ; Megnien et al., 1980 ; Perrodon and Zabek, 1991 ; Guillocheau et al., 2000). Thermal subsidence controlled the evolution of the basin at least until early Cretaceous times (Brunet and Le Pichon, 1982; Prijac et al., 2000). During late Cimmerian and late Aptian, two stages of emersion associated with erosion occurred (Fig. 2, Quesnel, 2003) as a result of both eustatic sea-level drop and distant influence of rift shoulder uplifts due to the North Atlantic rifting (Ziegler, 1990). The eastern basin margin definitively emerged and experienced weathering and erosion during the Cenozoic, allowing the progressive exhumation of the underlying Jurassic and Triassic sediments, which presently crop out in the study area (Fig. 1a).

2.2) Stratigraphy

In the part of the Lorraine coal Basin that was operated by HBL (Lorraine coal Basin company) close to the Saar, the stratigraphy was established with paleoflora sampled in coal mines and boreholes by HBL geologists and Laveine (1974). In the part of Lorraine without coal mines, the stratigraphy of seismic lines in Lorraine was done in using the logs of boreholes (Izart et al., 2005) and our interpretation. The paleoenvironments were determined from cores and logs of borehole by Izart et al. (2005). Various stratigraphic stages exist for the Carboniferous in continental western european coal basins (previous and recent stages), and in marine basins that are now the only stages accepted by the international commission on stratigraphy (Izart et al., 1998 and 2003 ; ICS, 2014). The continental stages and the marine stages are given below, with the marine stages in brackets. The Lorraine coal Basin is a limnic coal basin without connection with the sea, that is different of a paralic coal basin where are observed transgressive bands in the North France, Belgium and Ruhr basins (Izart et al., 2003). The Mid-German crystalline zone (Fig. 1c) contains continental coal basins : Lorraine and Saar-Nahe from Namurian to Permian (Korsch and Schäffer, 1995), but also other continental basins from Stephanian to Permian : Thuringian Forest and Saale (Roscher and Schneider, 2006 ; Schneider and Roscher, 2010).

In the Saar-Nahe coal Basin, Kelch and Reible (1976) described the stratigraphy of the Saar 1 borehole (Figs. 1b and 3) containing a thick series (5000m) of sandstones, coals and claystones deposited from Mississipian : Late Viséan and Namurian (Serpukhovian) to Pennsylvanian : Westphalian A or Langsettian and Westphalian B or Duckmantian (Bashkirian), Westphalian C or Bolsovian and Westphalian D or Asturian (Moscovian). In this basin, the Stephanian (Kasimovian) contains grey sandstone and claystone and the last coal seams, the Autunian (Gzhelian) red sandstone and limnic black shale, and the Permian

red sandstones and claystones dated Asselian to Wordian (Guadalupian) (Roscher and Schneider, 2006 ; Schneider and Roscher, 2010). The Permian also shows volcanic rocks (rhyolite, dacite and andesite) dated 296 to 293 Ma (Asselian to Sakmarian, Von Seckendorff et al., 2004).

In the Lorraine Coal Basin, the stratigraphy was described in detail by Donsimoni (1981) in a geological synthesis for the mining area of the basin located close to the Saar and for the extension of this basin towards Nancy in France (Fig. 1b). The Gironville borehole (Fig. 4, Tables 1 and 3) is in France the more complete borehole (4500m) from Late Viséan to Westphalian C. Numerous boreholes were only drilled in the Westphalian D and C (Table 1). The sediments and sequence stratigraphy of Westphalian C were studied by Fleck (2001), Fleck et al. (2001) and Izart et al. (2005) in using the boreholes Saulcy, Lorettes and Chaumont (Fig. 4) and the seismic sections EPLY 02, EPLY 06 and EPLY 07 (Fig. 5) for the lateral continuity of sequences. From Izart et al. (1998 and 2003), the Westphalian C and D were subdivided into three third order sequences (TOS) that correspond to the Neunkirchen, Geisheck and Petite Rosselle formations for the Westphalian C and four TOS that correspond to the Merlebach-Laudrefang conglomerate, Tritteling and Steinbesch formations for the Westphalian D (Fig. 4). The TOS from the Westphalian are constituted of fluvial conglomerate at the lower part, then a succession of high frequency sequences (HFS, 10m thick) constituted of fluvial conglomerate and sandstone, paleosoil, coal seam and lacustrine claystone. The coal seam thickness (1m to 10m) from the Westphalian D in Folschviller borehole (Fig. 1b) drilled by EGL for the coal gas is higher than coal thickness (1m to 2m) from the Westphalian C in Saulcy and Lorettes boreholes. Note that the succession of HFS is very important to understand for the oil and gas generation in coal seams and storage in coal seams and sandstones. The volcanism is represented in Lorraine by rhyolite (Figs. 1b and 2) that heated the Stephanian coals in Chevraumont and Forcelles boreholes. Close to the Metz fault, the Metz 1, Alzing, Hinckange and Saint Michel 1 boreholes exhibit Permian volcanic rocks (andesite, trachybasalte, Fig. 1b).

2.3) The tectonics of the Lorraine coal Basin

A new structural interpretation (Fig. 2) was proposed recently by Averbuch et al. (2012) considering the Lorraine coal Basin in the general context of the late evolution of the Variscan belt. This new model suggests that the Namurian and Westphalian formations between the Metz Fault and the Vosges border were deposited in a synorogenic basin developed, just south of the Rhenohercynian suture zone, on top of the Saxothuringian retro-wedge. Schäfer et al. (2000) described this Saxothruringian retro-wedge in the German Variscides based on Dekorp deep seismic profiles in Saar. Edel and Schulmann (2009) studied the Dekorp 88 and South Ecors-Dekorp deep seismic profiles that exhibit the Rheno-hercynian and Saxo-thuringian oceanic sutures, cut by Early Carboniferous magmatic bodies linked with a subduction. Westphalian sequences are generated under the compression by faults at the border or inside the basin. Folds and thrust faults in the basin (i.e. Merlebach and Morhange anticlines) would have occured initially by propagation at the surface of southeastward thrusting during the deposition of the Late Westphalian molassic sequence (the Asturian compressional phase). This contrasts with the classical interpretation of the basin that considers an extensional

control of the sedimentary sequences as soon as in Namurian times (Donsimoni, 1981). Schäfer et al. (2000) cited two stades of collision, the first during Viséan (340 Ma) and the second corresponding to folds and thrusts in the Lorraine coal basin during Moscovian (Westphalian C, 310 Ma). In this new tectonic scheme, normal faults would appear during the sedimentation of Stephanian and Autunian deposits reactivating at depth the previous thrust ramps and inducing the collapse of the back limb of the Late Westphalian anticlines. This transition at the Westphalian-Stephanian boundary between a compressional and extensional tectonic setting, emphasized in the basin by a major unconformity and the extensive deposition of a conglomeratic formation (the so-called Holz conglomerate), would sign at depth the onset of the delamination of the lithospheric roots of the Variscan belt (Averbuch and Piromallo, 2012).

These structures were slightly reworked again in Middle Permian times (between the Autunian and Saxonian) with the Saalian compressive phase exagerating the previous anticlines and the associated forelimb thrusts. This is particularly visible along the South Fault of the Sarrebrück anticline in Saar ; actually, in the Saar section (Fig. 3A after Geologische Ubersichtskarte, 1979), the South Fault is a complex thrust crosscutting the forelimb of the anticline with Stephanian layers in the direct footwall thereby suggesting a Permian age for the latest movements (Kelch and Reible, 1976 ; Geologische Ubersichtskarte, 1979 ; Henk, 1993). This Saalian compressive phase is however much less expressed in Lorraine (Pruvost, 1934) where no direct evidence of involvement of Stephanian layers in the thrust structures can be put forward. The general cross-section in Fig.3B (after Donsimoni, 1981) illustrates the overall structure of the part of the Lorraine coal Basin that was operated by HBL (Lorraine coal basin company) close to the Saar. Below the unconformable Triassic sequence, the Metz Fault separates the Devonian schists of the deformed Variscan substratum from the coal-bearing Westphalian deposits forming thereby the NW border of the Carboniferous basin. These deposits are involved in kilometric fold structures affected by both normal and thrust faults, i.e. from North-West to South-East : La Houve field, Merlebach anticline bordered to the south by the Hombourg Fault, Marienau syncline, Simon anticline, Landroff syncline, Alsting anticline and Sarreguemines syncline.

The EPLY 02, EPLY 06, EPLY 07, LOR 09 and L83C seismic lines (Fig. 5) exhibit the anticline with thrust from Saulcy and Pont-à-mousson that is the continuity of the Merlebach anticline, the Landroff syncline and the Morhange anticline with Morhange thrust, and finally the Sarreguemines syncline with Stephanian and Westphalian as far as the Adamswiller borehole (Fig. 1b). Note that the Westphalian D was deposited during the propagation of fold-thrust structures and that the faults in distension are located in the backlimb of the anticlines where Stephanian sediments were deposited. There is a major Asturian compressive phase and a limited Saalian compressive phase. In the TOUL 08, Toul 01-02 and Toul 10 seismic lines (Fig. 6), from West to East, the Devonian black schist is observed in Courcelles borehole, then the Metz Fault, then the Westphalian is observed in an anticline that is the continuation of the Pont-à-mousson anticline, drilled by the Gironville, Lerouville and Culey boreholes. The contact of Stephanian on the Westphalian was interpreted by Izart et al. (2005) as an unconformity. Then, a normal fault separates the Stephanian from the Westphalian that

is folded with inverse faults. Then, a syncline with Permian sediments (Germisay borehole) and volcanism and Stephanian sediments with coals in Jevoncourt, Chevraumont and Forcelles boreholes. The Carboniferous basin stops at west of the Toul 10 section on the Marne Fault (Fig. 1b).

3) Sampling and methodology

3.1) Boreholes and seismic lines

Numerous boreholes (Table 1) exist in France, among others : Merlebach (Figs. 1b, 3 and 4), Faulquemont and Folschviller (Fig. 1b), Saulcy (Figs. 1b, 4 and 5) in EPLY 02 seismic line, Lorettes (Figs. 1b, 4 and 5) in EPLY 06, Chaumont and Francheville (Figs. 1b, 4 and 5) in EPLY 07, Gironville (Figs. 1b, 4 and 5) in TOUL 08 and Culey (Figs. 1b, 4 and 6) in TOUL 10, located all on Merlebach and Saulcy, Pont-à-Mousson anticlines. In this study, the calibration was done in five seismic lines (Figs.1b, 5 and 6) : Eply 02-LOR 09, Eply 06 and 07, and Toul 08, and in fifteen boreholes (Fig. 1b, Table 1) in Lorraine: Chaumont 001 (Westphalian B and C), Chevraumont 1 (Permian and Stephanian), Culey 1 (Westphalian B, C and D), EST 433 (end in Triassic), Faulquemont 1 (Stephanian and Westphalian D), Forcelles 5 (end in Triassic), Francheville 1 (Permian, Stephanian and Westphalian B, C and D), Gironville 001 (Namurian and Westphalian A, B and C), Lerouville 1 (Stephanian and Westphalian C), Lorettes 001 (Westphalian B and C), Pont-à-Mousson 101 (Westphalian B and C), Rn 8 (end in Triassic), Saulcy 001 (Westphalian B and C), Trois-Fontaines 106 (Permian and metamorphic basement) and Vaxy 1 (Westphalian). The input data (thickness, depth, age and lithology) from Gironville is given in Table 3 and from all the boreholes as additional data. The seismic lines of this paper were transformed from time in depth in using the sonic log from each borehole. The transformation is better in the anticlines than in the synclines, because the boreholes are often drilled in the anticlines. The Rn 8 modelling was done in the Velaine sous Amance 49 (Va 49) borehole close to the Rn 8 because of the partial log of the Rn 8. The age (Ma) of stages are those given from ICS (2014).

3.2) Vitrinite reflectance and Rock-Eval data

Organic maturation data have been published in different studies but are consider together here to draw a general evolution of the basin. Data (VR) are from (1) Alpern (1969) and Durand et al. (1986) for the Gironville borehole, (2) Alpern (1969) for the Faulquemont borehole, (3) Blaise et al. (2011 and 2014) for EST 433 and Rn 8 boreholes and nearby outcrops, (4) Ménétrier (2005) calculated from Tmax data for the Chevraumont borehole, (5) Elixir confidential report from cores of Chaumont, Culey, Francheville, Gironville, Lorettes, Saulcy and Vaxy boreholes.

The values of T_{max} measured by Ungerer et al. (1986) in the Gironville borehole were not used in the modelling because there is no general law for the T_{max} as for the VR and it is

necessary to use a specific calibration curve for each OM and basin (Chadouli, 2013). The Total Organic Carbon (TOC), Hydrogen Index (HI=100*S2/TOC) and maximum Temperature of the S2 peak (T_{max}) measured by Fleck (2001) on coal and claystone samples from cores of Chaumont, Culey, Francheville, Lorettes and Saulcy boreholes (Table 5) were used for the organic matter characterisation. The Table 5 exhibits only some values of VR and depth of sampling published with Elixir permission because of the confidentiality of the Elixir report.

3.3) Apatite fission tracks

Apatite fission-track thermochronology is now a well-established method allowing the paleotemperature determination in the 60 – 110 °C range (Gallagher et al., 1998). Fission tracks correspond to defects caused by the spontaneous fission of 238U: fission fragments traveling across the crystal lattice damage the crystal order principally by electrostatic reactions. Atoms may return to their initial position when temperature is sufficient. Fission-track annealing experiments coupled with the study of well-constrained geological cases characterize the temperature domain where fission track are metastable: above 110 °C all tracks are reset, below 60 °C, tracks are preserved (Green et al., 1989). Paleotemperature can be determined by measuring fission track length of track parallel to the surface (confined track): track length is 14 – 15 µm for T < 60 °C and is ranging between 0 and 14 µm in the partial annealing zone (Green et al., 1989). Thermal modelling have been developed to extract from fission track data (age and length distribution) the thermal histories compatible with the data (Laslett et al., 1987 ; Ketcham et al., 1999, 2007).

Apatite fission-track data were obtained using the external detector method and zeta calibration (Hurford and Green, 1983). Samples were irradiated in the P1 facility of the Orphée reactor (Saclay, France) with a nominal flux of 1.37 1013 n.cm-2.s-1. Etching conditions are 5M HNO3 for 20 seconds at 20 ± 0.5 °C for apatite crystals and HF 40% for 20 minutes at 20 ± 1 °C for muscovite external detectors. Central ages are calculated using a ζ-value for the dosimeter glass CN5 of 359 ± 8 calibrated by multiple analyses of IUGS apatite (Durango, Fish Canyon) age standards (see Hurford, 1990). Only crystals with sections parallel to c-axis were analyzed. Confined track lengths have been measured using only Tints under a 100 x dry objective with a digitizing tablet linked via a drawing tube to the microscope. Angle to the c-axis is reported for each track. Thermal modelling has been carried out using the Ketcham et al. (1999) multicompositional annealing models and processed using AFTASolve (Ketcham et al., 2000 ; Ketcham, 2005) software. Dpar (diameter of the etch pits parallel to the c-axis) values and electron microprobe data have been measured to assess the chemical composition of the apatite crystals and to test the structural/chemical control of apatite on fission track annealing (Barbarand et al., 2003; Burtner et al., 1994; Green et al., 1986). Analytical procedures are similar to those described in Barbarand et al. (2013).

Fission-track ages have been acquired on six samples recovered from Lower Triassic sandstones sampled between 1886.1 m and 1989.5 m in Est 433 borehole in Meuse (Blaise et al., 2014) and one sample from Lower Triassic sandstone (Grès à Voltzia Formation) in Rn 8 borehole (Fig. 1b) located East of Nancy at a depth of 585m described in this paper.

3.4) Thermal and Hydrocarbon modelling

Table 2 presents the thermal conductivity, heat capacity and density of pure lithology. The same values were used by Hertle and Littke (2000) for the Saar coal Basin. The Tables 3 to 6 show all the stratigraphic and lithologic data used by the Petromod software 11.0 (Wygrala, 1988). The Table 3 exhibits the input data from the Gironville borehole. The input data from the other boreholes are presented in additional tables. The % of each lithology was calculated for each formation and the porosity laws for each lithology are those proposed in the software, similar to those from Le Soleuz et al. (2004). The sedimentary layers are decompacted by the software in using the backstripping technique from Sclater and Christie (2000). The burial history of some boreholes will be presented with the temperature history. The paleowater depth changes from 0m during the Carboniferous (only continental) to 50m during the Jurassic (marine Liassic and Callovian-Oxfordian claystone). The surface temperature was calculated on the basis of global mean surface temperature estimates (Wygrala, 1988). The best fit in calibration was obtained in testing diverse heat flows (HF) and eroded thicknesses (ET). The calibration was done in 1D from boreholes and then in 1D extraction from 2D in seismic lines (Figs. 7 to 9). The temperatures, hydrocarbon windows, organic matter (OM) transformation rates (TR), oil expulsion onset, oil and gas generation, storage and pathways were presented in the EPLY 02-LOR 09 and TOUL 08 seismic lines (Fig. 12 to 22, Tables 6 to 8). The organic matters and petroleum types were indicated in Figure 2. The source rocks (SR) consist of Westphalian, Stephanian and Upper Jurassic from type III and of Toarcian from type II. The reservoir rocks (RE) are composed of Permian and Triassic sandstones and Jurassic limestones and a seal rock (SE) is represented by the Upper Triassic (Keuper) evaporites. The hydrocarbons (HC) zones were modelled in 1D and 2D in using the Type III kinetics (Burnham and Sweeney, 1989 ; Sweeney and Burnham, 1990) for the Carboniferous after the HC data from Fleck (2001) and the Type II for the Toarcian (Behar et al., 1997). The oil and gas migration was calculated in using hybrid simulation with 2.00 log mD being the critical threshold value. Per default, a facies with a permeability of more than 2.00 log mD is considered a Flowpath layer, and migration is solved by buoyancy driven flow. Layers with a permeability of less than 2.00 log mD are Darcy layers where migration is solved according to Darcy's law.

4) Results and Discussion

4.1) Paleothermicity of the Mesozoic strata

The values of vitrinite reflectances (VR) and biomarkers from the Mesozoic on the EST 433 and Rn 8 boreholes and outcrops from Lorraine were measured by Blaise et al.

(2011 and 2014). Blaise et al. (2011) showed that the VR values from the Grès à Voltzia Formation in the Triassic are 0.65 in EST 433 borehole at a depth of approximatively 1900m and range from 0.5 to 0.6 in the Rn 8 borehole close to Nancy at a depth close to 500m (Fig. 1b). The VR values from the Toarcian and Hettangian are respectively equal to 0.3 and 0.47 in Essey and Solgne outcrops near Nancy. The oil window begins in the Keuper in Lorraine. The maturity of the Mesozoic decreases from West (EST 433) to East in Lorraine in relationship with the decrease of the thickness of the Cretaceous cover. Blaise (2012) and Blaise et al. (2014) modelled the paleotemperatures in the EST 433 borehole (Fig. 1b) by Petromod software 11.0 and calculated a heat flow of 65 mW/m^2 at the beginning of Permian, followed by an exponential decrease towards a mean present day value of 55 mW/m^2, and a Cretaceous eroded thickness of 322m including 22m for Early Cretaceous constituted of sandstone, limestone and claystone and 300m for Late Cretaceous constituted of chalk. New data on fission-tracks and a modelling from the Rn 8 borehole using the VR measured by Blaise et al. (2011) are proposed in this paper.

Fission-track ages are ranging between 41 ± 5 and 79 ± 14 Ma in EST 433 borehole in Meuse and are characterized by a low P ($\chi 2$) indicating a relative large variation of single grain ages. This variation is poorly controlled by chemistry or structure estimated by the Dpar parameter although oldest grains show largest Dpar which confirm the role of chemistry or structure on the track annealing (Carlson et al., 1999; Barbarand et al., 2003). All grains (118 grains) characterize a main population at ~ 50 Ma; this population represents more than 75 % of the grain for all samples (except one where it represents 56 %). Mean horizontal confined track lengths are ranging between 10.5 and 11.8 µm and the mean track for all samples is 10.9 µm with a standard deviation of 1.8 µm.

Considering that all samples have been collected in a small depth interval (~ 103 m equivalent to ~ 3 °C considering present-day gradient), that no major differences exist among samples and that temperature precision of fission track method is less than 5 °C, all these samples can be considered together to extract a robust thermal history assuming a mean age of 66 ± 44 Ma and a mean length of 10.9 µm.

From Rn 8 borehole sample, fission-track age is 120±10 Ma characterizing a significant post depositional heating. A horizontal confined mean track-length of 12.4±0.2 µm (standard deviation of 1.4 µm) and a relative large dispersion of the ages (Fig. 7A and B) illustrate a slow cooling after the maximum temperature. Thermal history modeling has been carried out assuming (1) the stratigraphic age of the sample: 250-247 Ma, (2) a present-day minimum burial of 585 meters corresponding to an additional paleotemperature of 12 to 23°C assuming a paleogradient of 30±10°C/km, (3) a present-day temperature of 29°C. Modeling has been processed with HeFTy (Ketcham, 2005) using the Ketcham et al. (2007) annealing model. Modelling result shows that a maximum burial temperature of 100±10°C occurred during the Late Jurassic, compatible with the deposition of a thick Jurassic cover (Fig. 7C). The cooling which succeeds is relatively rapid during the Early Cretaceous and is moderate up to the present-day temperature. No Upper Cretaceous heating is required by the modelling.

Two scenarios were tested from the 1D modelling of the Rn 8 borehole (Fig. 8): scenario A with a Mesozoic erosion at the end of Cretaceous and scenario B with an erosion at the beginning of Early Cretaceous for the Late Jurassic and at the end of Cretaceous for the Mid-Jurassic, Early Jurassic and Triassic, with a heat flow (HF) from 60 mW/m^2 for the Early Permian followed by an exponential decrease to 40 for the Recent, and Cretaceous erosion thickness (CET) : 122m and 322m to test the decrease of Cretaceous thickness towards East. The two erosion scenarios cannot be separated by the VR calibration. The two values of the CET present the same good calibration, the thickness is certainly between 122m and 322m in the Rn 8 borehole, because the VR range from 0.5 to 0.6. But if we compare the TF values with a fission-track age at 120±10 Ma and a maximum burial temperature at 100±10°C with the lateral range of the temperature 100°C (in green) in the burial and temperature history at the Triassic base, the new data on fission-tracks from the Rn 8 borehole allow us to check the low Cretaceous thickness in the eastern part of Lorraine and the scenario B.

Modellings were also done in boreholes that were drilled through the Mesozoic and Paleozoic : Chaumont, Chevraumont, Culey, Faulquemont, Forcelles, Francheville, Gironville, Lerouville, Lorettes, Pont-à-Mousson, Saulcy and Vaxy (Fig. 9). For all these boreholes from 1D modelling (Fig. 10), the better calibration is obtained for a HF from 60 mW/m^2 for the Early Permian followed by an exponential decrease to 40 for the Cenozoic and Recent taking into account a VR equal to 0.55 in Buntsandstein measured in the eastern part of the Lorraine (Blaise et al., 2011) and the vitrinite reflectances from the Paleozoic. According to the comparison with the VR range, the CET is equal to 320m for Gironville, 100m for Saulcy and 0m for Vaxy and Faulquemont. For Gironville and Saulcy extracted from 2D modelling (Fig. 10), the better calibration is for the case of HF equal to 55 mW/m^2 at the base of Triassic, 50 at the top of Cretaceous and 40 for the recent time or 50 mW/m^2 all the time. If diverse ET are compared for the same HF within the VR range (Figs. 9 and 10 and Table 7), the better calibration is observed for a Cretaceous ET lower than 320m in Gironville, 100m in Saulcy and 0m in Vaxy and Faulquemont. Blaise (2012) modelled a cross-section from the centre of the Paris Basin (Donnemarie borehole) to Vosges (Raon-sur-Plaine), and showed that the Cretaceous cover decreases from 322m in Gironville, 100m in Forcelles to 0m in the Vosges. After these data, a limit between thick (>100m) and thin Cretaceous deposits (100m to 0) was drawn on the maps (Fig.1a and b). The Cretaceous ET is equal to 320m in the western part of the Lorraine in EST 433 (Blaise et al., 2014), Trois-Fontaines (Blaise, 2012), Culey (Fig. 9), Chevraumont (Fig. 9), Francheville (Fig. 9) and Gironville (Figs. 9 and 10), 100m in Saulcy and Forcelles (Blaise, 2014), 0m in Faulquemont and Vaxy (Fig. 9 and Table 7) after the VR range. The sensitivity on ET is equal to 300m in Gironville (Fig. 11) and EST 433 (Blaise et al., 2014) and 50m in Saulcy and Vaxy (Fig. 10). The difference between a small erosion of Jurassic top during the Early Cretaceous and the erosion of Cretaceous and Jurassic top during the Cenozoic is not quantifiable in these 1D modellings. But, the existence of the erosion surface of Early Cretaceous was argumented by Le Roux (1980, 2000) and Le Roux and Harmand (2003) and by the datation of this surface by Quesnel (2003) and Theveniaut et al. (2007) in Lorraine on the Jurassic (« Borne de Fer »). The Mesozoic ET (Table 7) ranges from 433m to 1915m and increases from West to East after the erosion surface. According to Lucazeau and Vasseur (1989) the mean present-day

surface HF is around 60-70 mW/m^2 in the Paris Basin, decreases in Lorraine as our result, then increases in Vosges (90) and after Lampe and Person (2002) in central Rhine Graben (110-130). Subsidence in the intracratonic Paris Basin was driven by the lithosphere thermal relaxation after the general collapse of the Variscan belt (Prijac et al., 2000). Thus, the basal HF has decreased exponentially since the Late Carboniferous/Early Permian pulse (Le Solleuz et al., 2004).

Fluid inclusions were studied by Blaise (2012) and Blaise et al. (2014) in siliceous overgrowth around quartz from Buntsandstein conglomerate in EST 433 borehole, halite from Keuper of Varangeville salt mine and calcite veins from Jurassic limestones of the Gondrecourt graben. The entrapment temperatures were calculated and are similar to the temperatures calculated by modelling and fission tracks for Jurassic, slightly higher for Keuper and lower than maximal burial temperature for Buntsandstein samples. Authigenic illites in Buntsandstein are dated Early and Late Jurassic by K-Ar (Blaise, 2012) and are tentatively interpreted to be relative to the North Atlantic ocean opening.

4.2) Paleothermicity of the Paleozoic strata

VR values (Table 6) range in the Paleozoic : (1) from 0.7 (High volatile bituminous coal) to 4.4 (anthracite) at 5675m in the Gironville borehole (Durand et al., 1986 ; Ungerer et al., 1986), (2) from 1.4 to 3 in the Chevraumont borehole (Menetrier, 2005) in the Stephanian coal close to the Permian rhyolite, (3) from 0.7 to 0.8 in coal and claystone samples from cores of Chaumont, Lorettes, Saulcy and Vaxy boreholes (Elixir data, Table 6) for the Westphalian C, (4) from 0.7 to 1 in the Faulquemont borehole for Westphalian D and C coals (Alpern, 1969). Note that the highest VR values in Gironville borehole were not taken into account in our modelling because new VR measurements from Elixir showed that there were measured on inertinite. Courel and Liu (1991) studied the geothermal history of intermontane coal basins in French Central Massif and Lorraine with a section and a map of present temperatures in the HBL area. Menetrier (2005) and Menetrier et al. (2005) published values of heat flows and eroded thickness for Gironville, Culey and Chevraumont boreholes.

Our modelling results show that the heat flows (HF, Tables 6 and 7) range from 50 during the Westphalian to 60 mW/m^2 for the Stephanian and Permian followed by an exponential decrease to 40 for the Cenozoic and Recent in the Lorraine boreholes that are located eastward on the Carboniferous Basin. The eroded thickness must take into account three well-defined erosion phases during : the Permian, the Early Cretaceous and the Cenozoic. All the phases were tested in 1D modelling and only the third was drawn in the 2D modelling because the paleozoic eroded thickness is not very high after the 1D. The Figure 9 exhibits all the curves of calibration for all the boreholes. Diverse HF and ET were tested for Gironville in 1D (Fig. 9) and extracted from 2D in TOUL 08 (Fig. 10, Table 6). The Gironville borehole is the best for the calibration because the VR were measured through out the Westphalian. For all modellings from 1D (Fig. 10), the calibration is the best for a HF equal to 50 mW/m^2 during the Westphalian and 60 during Stephanian and Permian. However the highest value of HF is equal to 400 mW/m^2 during the Permian (Fig. 9) from the Chevraumont borehole

because of the rhyolite heating. For Gironville and Saulcy extracted from 2D (Figs. 9 and 10), the calibration is the best for the case of HF equal to 50 mW/m^2 during the Westphalian, 60 during the Stephanian and Permian, or 50 mW/m^2 all the time and the calibration was no good for 40 mW/m^2. For Lorettes and Chaumont extracted from 2D, the HF also range from 45 to 50 mW/m^2 (Fig. 9). There is no difference of HF between the 1D and 2D modelling because of a low Paleozoic eroded thickness. A sensitivity of HF calibration is equal to 5 mW/m^2 by comparison of the curves with HF variable or equal to 50 from Gironville (Fig.10). This value is similar to this described by Blaise et al. (2014) from EST 433 borehole. The values of heat flows are close of those published by Menetrier (2005) and Menetrier et al. (2005) for Gironville (63 mW/m^2), Culey (58), Francheville (55) and Chevraumont (400 during the Permian) boreholes with an uncertainty of 10%. These HF are similar or lower than in the Saar coal Basin. Littke (2000) and Hertle and Littke (2000) modelled the paleotemperatures in the Ruhr and Saar Basins. For the Saar Basin, they used sixteen boreholes, including the Saar 1 (Fig. 1b, section 1) and Meisenheim 1 (East Saar) boreholes and one section across the Saar Basin. Maps with vitrinite reflectances, heat flows (HF) and eroded thicknesses (ET) were drawn. The coalification is syn-kinematic in Saar Basin, the vitrinite reflectances isolines cut the stratigraphic limits. In Saar 1 and Meisenheim 1 boreholes, the HF are respectively equal to 70 and 60 mW/m^2 and eroded thickness of Paleozoic 2000m and 3600m and Mesozoic (Triassic and Jurassic) 1200m. The intra-Westphalian D compression phase does not seem affect the 2D modelling, because the Gironville borehole is located in the eastern limb of an anticline without thrust, and the Saulcy and Vaxy boreholes are located in an anticline closure with thrust in the eastern limb. The thrusts are intra-Westphalian D with a low displacement (200m in Saulcy anticline and 1000m in Morhange anticline) and sealed quickly by the Stephanian. In this case, balanced sections used by Faure et al. (2004) in their modelling are not necessary and will not bring a best modelling of heat flow and paleotemperatures. The post-folding coalification that cut the stratigraphic limits is the more significant in our sections as noted by Courel and Liu (1991) for the HBL sector, where according to these authors the pre-folding coalification is still recognizable. So the coalification is different from the Ruhr coal Basin where the pre-folding coalification exists only with VR curves parallel to the stratification (Teichmüller and Teichmüller, 1971 and Littke et al., 2000). The HF were medium (50 mW/m^2) in Lorraine during the Westphalian in a synorogenic basin developed on the top of the Saxothuringian retro-wedge, then the HF (60 mW/m^2) increased during the extension phase of the Stephanian and Permian. The HF values of the Lorraine coal Basin correspond to the HF range (40 to 80 mW/m^2) from the collisional belt lower than the HF range (60 to 100 mW/m^2) from the extension basin (Allen and Allen, 1990).

The high HF during the Carboniferous from the Saar coal Basin would be explained by a crustal thickness of 30-40 km below this basin according to Hertle and Littke (2000). But the crustal thickness is 20-30 km below the Saar according to Schäfer et al. (2000) and below the Lorraine according to Edel and Schulmann (2009). The difference of HF between Saar and Lorraine cannot be due to the thermal conductivity of sediments because we used the same values for pure lithology. Le Soleuz et al. (2004) calculated HF in the Paris Basin in the case of an extensional collapse of the hercynian orogeny during the Carboniferous and Permian or a delamination of the lithosphere. However the two scenarios cannot be separated by their

modellings. The two modellings gave a present-day average surface heat flow respectively equal to 68 and 69 mW/m^2 with a lithospheric thickness of 120 km and a crustal thickness of 36 km in Lorraine. Hertle and Littke (2000) wrote that short hot fluids cannot be excluded in the Saar coal Basin close to the faults, but are difficult to prove because their duration is too short to change the OM and there is no data on fluid inclusions in Paleozoic rocks.

The Paleozoic ET (Table 7) ranges from 0m to 1200m in 1D modelling and depends of the borehole location on syncline or anticline, and erosion degree of anticline. The uncertainty on Paleozoic ET is difficult to measure because of the short duration between deposition of formation during Westphalian and the erosion during Stephanian or Permian, which produces a small impact of OM maturity from Paleozoic. There is no change in maturity if a thickness of 600m is added to the Westphalian in Gironville (Fig. 10). The Paleozoic ET in Lorraine is lower than in Saar (Littke, 2000 and Hertle and Littke, 2000), however Mesozoic ET in Saar was probably underestimated. Note that in Lorraine a continuity and not a big jump of VR between the top of Carboniferous (VR=0.7) and the Triassic base (VR=0.6) is observed, the Paleozoic ET was therefore weak. The boreholes are often located on anticlines where the deposition of Stephanian and Permian was weak.

Maximal paleotemperatures (MT) and Recent temperatures (Figs. 11 and 12) were calculated in 2D and 1D modelling in using the Type III kinetic (Sweeney and Burnham,1990). The burial and temperature history was presented in Fig. 8 for Rn8 borehole and Fig. 12 for Gironville, Saulcy and Vaxy boreholes from 1D modelling. The Figures 8 and 12 show that the maximal temperature is located at the top of Jurassic during the last sedimentation period. However, the maximal temperature will be Jurassic by TF from the Rn 8 borehole. The recent temperature gradient was measured in Lorraine: 30°C/km in EST 433 (Blaise et al., 2014), 40°C/km in Gironville (Ungerer et al., 1986) and 30°C/km in syncline and 50°C/km in anticline from the HBL area (Courel and Liu, 1991). A MT of 50°C was reached at the top of Cretaceous for the Callovo-Oxfordian, 75°C for the Toarcian and 100°C for the Buntsandstein in the EST 433 borehole (Blaise, 2012 ; Blaise et al., 2014). The MT of 80°C was reached at the top of Jurassic for the base of Buntsandstein and 100°C for the Westphalian C in Gironville, Culey, Lorettes, Saulcy and Rn 8 boreholes if there is no erosion at the end of Jurassic. The sensitivity on temperatures is equal to 5°C after Blaise et al. (2014).

5) Consequences for the petroleum system in the Lorraine coal Basin

As the initial Westphalian HI ranges from 100 to 200 mg HC/g TOC (Table 6), the organic matter from coals and claystones is of type III (Espitalié et al., 1977 and 1985). Some rare coal HI can reach the value of 300 because of the presence of hydrogen-rich vitrinite and exinite (spores). Rare dark lacustrine claystones are known in the Geisheck formation (Westphalian C) from 1000 to 960m in the Lorettes borehole (Fleck, 2001). These lacustrine claystones are not of type I, but of type III with a HI from 126 to 144. However, the steranes come from a mixture of higher plants (C_{29}) and algae (C_{27}) in these limnic samples. There is no proof of Autunian lacustrine claystones in Lorraine as in the Saar coal Basin where the HI values range from 100 to 500 (Izart et al., 2012). In the column HI from Table 6, the initial HI

values used in the modelling are written and in brackets the measured HI values that increased, then decreased with the OM heating (Espitalié et al., 1977 and 1985). The TOC value for a formation takes into account the % and the TOC of coals and claystones in this formation.

The hydrocarbons (HC) zones were modelled in 1D and 2D in using the Type III kinetics (Burnham and Sweeney, 1989 ; Sweeney and Burnham, 1990) for the Carboniferous after the HC data from Fleck (2001). The western part of the Lorraine presents immature organic matter in all the Jurassic rocks and oil window in the Triassic rocks in EST 433, Trois-Fontaines and Culey boreholes. The eastern part of the Lorraine (Fig. 13, Table 7) exhibits immature organic matter in the Jurassic and Triassic rocks, oil window in the Permian, Stephanian and Westphalian D, gas window in Westphalian B-C and overmature in Namurian-Westphalian A.

The OM transformation rate (TR) was also calculated. In the Lorraine (Table 7), the TR is equal to 20% in Stephanian, 50-80% in Westphalian D and C, 90% in Westphalian B, 100% in Namurian-Westphalian A.

The expulsion onset of oil and gas (Table 8) in the Westphalian is the Permian (300Ma) in all the sections of the Lorraine Basin, and for the Stephanian, it is the Late Jurassic (140Ma).

The oil and gas generation masses (Mtons/km^3 of rock, Table 8) are respectively for the Westphalian A, B and C equal to 0.5-5 and 0.5-10 in the EPLY 02-LOR 09 seismic lines (Fig. 14) and equal to 1-8 and 1-20 in the TOUL 08 seismic line (Fig. 15). The difference of generation between the formations and seismic lines can be explained by the diverse TOC values and HC zones, and also the location in anticline (high value) and syncline (low value). The Tables 6 and 7 present the results for diverse HF and ET.

The oil and gas storage masses (Mtons/km^3 of rock, Table 8) for the Westphalian A, B and C are respectively equal to 0-0.5 and 0-0.25 except 50 in some traps along faults in anticlines in the EPLY 02-LOR 09 seismic lines and equal to 0-1 and 0-0.25 except 1 in some traps in eastern anticline in the TOUL 08 seismic lines. These values of oil and gas storage masses are low except along the faults in anticline. The hydrocarbures are stored else in sandstone reservoirs from the Carboniferous or Triassic, or in coal and claystone source rocks from the Carboniferous. The Tables 7 and 8 present the results for diverse HF and ET. The values of unconventional oil and gas volumes estimated by Elixir (Elixir, 2011) in their Lorraine permit (5360 km^2) for the Carboniferous are respectively 2.6 10^{10} m^3 and 1.84 10^{13} m^3, and the conventional gas in Carboniferous and Triassic reservoir 6.23 10^{10} m^3. The unconventional gas mass corresponds to 0.5 Mtons/km^3 of rock. The values of contingent and prospective CBM volumes estimated by EGL (Beicip Franlab, 2012) in their Lorraine permits (1150 km^2) is equal respectively to 1.7 and 1.9 10^{11} m^3. The CBM masses correspond respectively to 18000 and 25000 tons/km^3 of rock. Our modelling from Faulquemont borehole located close to the Folschviller borehole shows a gas storage equal to 0.01 Mtons/km^3 of rock similar to EGL estimation. The range of our calculated storage values are often intermediate with the estimations from Elixir and EGL gas companies. However note that it is

difficult to calculate a precise estimation of the reserves because of the heterogeneity of coal % in the formations and oil and gas storage masses in our modelled sections.

To check the feasibility of CBM exploitation in Lorraine, two criteria are important : the adsorption capacity of coal for the methane storage and the cleat system inside the coal for the methane storage and desorption during exploitation. The adsorption isotherm from a coal of La Houve with a VR equal to 0.74 shows a maximum adsorbed gas quantity q_{mc} equal to 0.54 mmol/g_{DAF} (Garnier et al., 2011 ; Gaucher et al., 2011 ; Charriere et al., 2010). For comparison, the q_{mc} from a coal of Monsacro Basin (Spain) with VR equal to 0.98 and an anthracite of Jerada Basin (Morocco) with a VR equal to 3.65 are respectively equal to 0.74 and 1.53 mmol/g_{DAF}. These values correspond respectively to 10, 13 and 31 m^3/ton of coal. These high values in anthracites were also observed in Donets coal Basin (Ukraine) by Alsaab et al. (2009). The Fig. 16 A shows the curve adsorption capacity vs. VR built after these data. These values are lower than those (Fig. 16B) measured by Hildenbrand et al. (2006) in Campine coal Basin (Belgium) and Ruhr coal Basin (Germany), peculiarly for the low VR. Juch et al. (2004) showed in the Ruhr coal Basin the part of subsidence phase on methane adsorption in the shallow depths with storage in coal and desorption in the deeper depths with migration towards the top. The inverse situation is observed during the uplift phase with migration towards the surface and atmosphera in the shallow depths and storage in the deeper depths. In Lorraine, two cycles of subsidence-uplift during Carboniferous and Permian, and during Mesozoic and Cenozoic explain the methane storage during the Carboniferous and Mesozoic, followed by desorption in the shallow depths during the Permian and Cenozoic. The Fig. 16 C, D and E show the change of adsorption capacity of coal in the Gironville, Saulcy and Faulquemont boreholes. These figures were built after the VR data obtained by our Petromod modelling and the Figure 16A on the burial history as done by Juch et al. (2004). An adsorption capacity from 10 to 15 m^3/ ton of coal is observed in the Westphalian C and B from Gironville and Saulcy boreholes and of 10 m^3/ ton of coal in the Westphalian D from Faulquemont borehole. Hildenbrand et al. (2006) calculated adsorption capacity cuves vs. depth for different VR. This capacity decreases from 20 m^3/ton at 1 km to 16 m^3/ton at 3 km for a VR equal to 1. The gas produced in the Folschviller borehole close to the Faulquemont borehole showed that CBM exploitation is possible in the EGL permits. A gas storage of 10 m^3/ ton of coal with 96% methane was observed in the Westphalian D with 8% of coal and VR from 0.84 to 0.93 and depth from 1 to 1.5 km in the Folschviller borehole (EGL, 2012). Alsaab et al. (2008b) showed by artificial maturation that a coal of VR equal to 1 presents a % C_1, C_2, C_3 and C_4 equal respectively to 26, 5, 35 and 21. The highest methane value in this coal can be only explained at these VR by gas migration from coals located below in Westphalian C and B. EGL drilled this borehole with lateral horizontal drains inside coal seams to improve the surface of gas desorption and used water pumping inside the coal that decreases the pressure and increases the gas desorption (EGL, 2012). Application of X-ray computed tomography allowed to analyse types of cleats (Fig. 17) and cleat spacing and cleat aperture (Fig. 18) in Lorraine coals in using Mazumber et al. (2006) technics. The Fig. 17 exhibits from a coal of Wesphalian D of the Tritteling 1 borehole face cleats (dominant, ellipsoid geometry, tensile origin) and butt cleats (curvilinear, shearing cleat from compressive and strike-slip origin) with the same orientation than the fractures (N-S and W-

E) measured in coals in Faulquemont coal mine and boreholes by Bles and Lozes (1980). These fractures are parallel to the faults in the Faulquemont area. The cleat spacing and aperture (Fig. 18) of cleats will allow a best gas desorption after the criteria of Rodriguez et al. (2014). The volume of cleat intersected in the biggest and smallest connected volumes and the volume of cleat detected were calculated with Aviso software on snap shots (Fig.18). The biggest connected cleat volume is shown in light blue and the smallest connected cleat volumes are show by different colors. Spheres (circles) correspond with centers of individual fractures. The connectivity between cleats is equal to Gcf = total volume of cleat intersected in the biggest connected volume / total volume of cleat detected. In our sample, Gcf = 1.78 10^{12} μm^3 / 1.90 10^{12} μm^3 = 93,7%. This result corresponds to a good connectivity. The presence of these natural cleats will avoid to use hydraulic fracturation in coals, and allows to know the directions of horizontal drains (N-S and W-E) to bore in the coal seam to increase the gas desorption.

The oil and gas migration can be also modelled by Petromod in the EPLY 02- LOR 09 seismic lines (Fig. 19) and the TOUL 08 seismic line (Fig. 19). The oil and gas of the Carboniferous rocks in Lorraine migrate upward along faults and across sediments from syncline to anticline to the Westphalian top, Stephanian, Buntsandstein and Muschelkalk or escapes laterally towards the East. The Keuper halite constitutes a barrier for the migration. As the expulsion onset began in Permian, a great part of generated oil and gas during the Carboniferous was lost. Some traps formed by small horst capped by impermeable claystone stored the oil in Forcelles and gas in Trois-Fontaines in the Muschelkalk dolomite or sandstone. These results complete for the Lorraine Basin the migrations described by IFP in the Paris Basin (Espitalié et al., 1987 ; Poulet and Espitalié, 1987) and checked in the 2D modelling of the Paris Basin (Blaise, 2012).

6) Conclusion

This paper proposes to reconstruct the thermal evolution of the Paleozoic and Mesozoic rocks from the Lorraine coal Basin and the consequences on hydrocarbons generation and storage, using a new tectonic interpretation. From Averbuch et al. (2012), a folding with reverse faults (Merlebach and Morhange) occured during the deposition of the Westphalian D corresponding to the Asturian compression phase. Normal faults in distension occured during the sedimentation of Stephanian and Autunian between the anticlines. The Saalian compression phase known in Saar is less expressed in Lorraine.

First of all, the paleothermicity during the Mesozoic was calculated, then during the Paleozoic in 1D and 2D modellings. Blaise et al. (2014) calculated paleotemperatures at the base of Triassic (100°C), variable Mesozoic heat flows (HF=55 to 40 mW/m^2) and Cretaceous eroded thickness (CET=322m) in EST 433 borehole (West Lorraine). And for this paper, the paleotemperatures, variable HF (60 to 40 mW/m^2) and eroded thickness for the Cretaceous (CET), Mesozoic (MET) and Paleozoic (PET) were calculated by Petromod software in East Lorraine. There is not a large gap of vitrinite reflectance and paleotemperature in East Lorraine between the Triassic base (respectively 0.55 and 80°C) and the top of Carboniferous

(respectively 0.7 and 100°C), the PET is small (lower than 1200m) and the CET is lower 300m and decreases to 0m eastward. The new data on fission-tracks from the Rn 8 borehole allow us to check the low Cretaceous thickness in the eastern part of Lorraine. The PET is small because of the compression phase during the Westphalian D followed by erosion at the base of Stephanian and weak extension during Stephanian and Permian in Lorraine (Averbuch et al., 2012). The HF agree well with the periods of compression and extension during the Paleozoic and extension during the Mesozoic.

Hydrocarbon generation has been also modelled. The eastern part of the Lorraine exhibits immature rocks in the Jurassic and Triassic rocks, oil window in the Permian, Stephanian and Westphalian D, gas window in Westphalian B-C and overmature in Namurian-Westphalian A. The oil and gas generation masses (Mtons/km^3 of rock) are respectively for the Westphalian A, B and C equal to 0.5-8 and 0.5-20 in the EPLY 02-LOR 09 and TOUL 08 seismic lines. The oil and gas storage masses (Mtons/km^3 of rock) for the Westphalian A, B and C are respectively equal to 0-0.5 and 0-0.25 except 50 in some traps along faults in anticlines in the EPLY 02-LOR 09 seismic lines and except 1 in some traps in eastern anticline in the TOUL 08 seismic line. The oil and gas of the Carboniferous rocks in Lorraine migrate upward along faults and across sediments from syncline to anticline to the Westphalian top, Stephanian, Buntsandstein and Muschelkalk or escapes laterally towards the East. The Keuper halite constitutes a barrier for the migration. As the expulsion onset began in Permian, a great part of generated oil and gas during the Carboniferous was lost. Some traps formed by small horst capped by impermeable claystone stored the oil in Forcelles and gas in Trois-Fontaines in the Muschelkalk dolomite or sandstone. The Lorraine coal basin is therefore a target for coal gas, which explains the drillings for coal gas from 1960 to now in Lorraine by ESSO, SNPA, Conoco Phillips (Dupont De Nemours), EGL and Elixir companies (Table 1). The methane adsorption capacity of coal and the presence of a natural cleat system inside coal with a good connectivity will allow a good CBM exploitation in this basin without hydraulic fracturation.

Acknowledgments

We thank ANDRA, Conoco Phillips and Elixir for their permission to use the seismic lines TOUL, EPLY and LOR that we interpreted, and Schlumberger for the use of Petromod software. Elixir and European Gas Limited (EGL) are thanked for the provision of their reports on VR, gas and oil storage masses. GDF is thanked for the autorisation of sampling of sandstone cores from Rn 8 borehole. Olivier Averbuch is thanked for his help in discussing the tectonics part of this paper and Thomas Blaise for his help in the 2D modelling with Petromod software.

References

Allen, P.A., Allen, J.R., 1990. Basin analysis : principles and applications. Blackwell scientific publication, 386p.

Alpern, B., 1969. Le pouvoir réflecteur des charbons français. Applications et répercussions sur la théorie de A. Duparque. Annales de la Société Géologique du Nord, LXXXIX, 2, 143-166.

Alpern, B., Choffe, M., Lachkar, G., Liabeuf, J.-J., 1969. Synthèse des zonations palynologiques des bassins houillers de Lorraine et de Sarre. Revue de Micropaléontologie, 4, 217-221.

Alsaab, D., Elie, M., Izart, A., Sachsenhofer, R.F., Privalov, V.A., 2008a. Predicting methane accumulation generated by humic carboniferous coals in the Donbas fold belt (Ukraine). AAPG Bulletin 92, 8, 1029-1053.

Alsaab, D., Elie, M., Izart, A., Sachsenhofer, R.F., Privalov, V.A., Suarez-Ruiz, I., Martinez, L., 2008b. Comparison of hydrocarbon gases (C_1-C_5) production from Carboniferous (Donets, Ukraine) and Cretaceous (Sabinas, Mexico) coals. International Journal of Coal Geology 74, 154-162.

Alsaab, D., Elie, M., Izart, A., Sachsenhofer, R.F., Privalov, V.A., Suarez-Ruiz, I., Martinez, L., Panova, E.A., 2009. Distribution of thermogenic methane in Carboniferous coal seams of the Donets coal Basin (Ukraine) : « Applications to exploitation of methane and forecast of mining hazards ». International Journal of Coal Geology 78, 27-37.

Averbuch O. and Piromallo C., 2012. Is there a remnant Variscan subducted slab in the mantle beneath the Paris basin ? Implications for the late Variscan lithospheric delamination process and the Paris basin formation. Tectonophysics 558-559, 70-83. Doi : 10.1016/j.tecto.2012.06.032.

Averbuch O., Piromallo C., Izart A., 2012. A model of heterogeneous delamination of the Variscan lithospheric roots in Northern France by Late carboniferous-Early Permian times : implications for the Late Variscan orogenic collapse and the Paris basin development. In Length scales, time scales and relative contribution of Variscan orogenic events to the formation of the European crust. Special Meeting of the French and Italian Geological Societies, Sassari, Italy. Géologie de la France, 2012, n°1, pp. 58.

Barbarand, J., Hurford, A.J., Carter, A., 2003. Variation in apatite fission-track length measurement: implications for thermal history modeling. Chemical Geology 198, 77 – 106.

Barbarand J., Quesnel F., Pagel M., 2013. Lower Paleogene denudation of the Upper Cretaceous cover of the Morvan massif and south eastern Paris Basin (France) revealed by AFT thermochronology and paleoweathering study. Tectonophysics 608, 1310-1327.

Behar, F., Vandenbrouke, M., Tang, Y., Marquis, F., Espitalie, J., 1997. Thermal cracking of kerogen in open and closed system: determination of kinetic parameters and stoichiometric coefficients for oil and gas generation. Organic Geochemistry 26, 321 – 339.

Beicip Franlab (2012). Audit de l'estimation des ressources sur les permis de EGL en lorraine et Nord-Pas de Calais. Rapport à la demande de EGL.

Blaise, T., 2012. Histoire thermique et interactions fluides-roches dans l'Est du Bassin de Paris. PHD Thesis, Lorraine University, 324p.

Blaise, T., Izart, A., Michels, R., Suarez-Ruiz, I., Cathelineau, M., Landrein, P., 2011. Vertical and lateral changes in organic matter from the Mesozoic, eastern Paris Basin (France): Variability of sources and burial history. International Journal of Coal Geology 88, 163-178.

Blaise, T., Barbarand, J., Kars, M., Aubourg, C., Izart, A., Pagel, M., Boiron, M.C., Cathelineau, M., Gautheron, C., Ploquin, F., El Albani, A., Michels, R., Pozzi, J.P., Janots, D., Brigaud, B., Landrein, P., 2014. Reconstruction of low burial (<100 °C) in sedimentary basins: a comparison of geothermometers sensibility in the intracontinental Paris Basin. Marine and Petroleum Geology 53, 71-87.

Bles, J.L., Lozes, J., 1980. Gazéification in situ du charbon, site de faulquemont, étude structural. BRGM report 80SGN427GEO, 28p. and 20 annexes.

Bourquin, S., Robin, C., Guillocheau, F., Gaullier, J.M., 2002. Three-dimentional accomodation analysis of the Keuper of the Paris Basin: discrimination between tectonics, eustasy and sediment supply in the stratigraphic record. Marine and Petroleum Geology 19, 469 – 498.

Bourquin, S., Peron, S., Durand, M., 2006. Lower Triassic sequence stratigraphy of the western part of the Germanic Basin (west of Black Forest): Fluvial system evolution through time and space. Sedimentary Geology 186, 187 – 211.

Bourquin, S., Guillocheau, F., Peron, S., 2009. Braided river within an arid alluvial plain (example from the Lower Triassic, western German Basin): recognition criteria and expression of stratigraphical cycles). Sedimentology 56, 2235 – 2264.

Brunet, M.F., Le Pichon, X., 1982. Subsidence of the Paris Basin. Journal of Geophysical Research 87, 8547 – 8560.

Burnham, A.K., Sweeney, J.J., 1989. A chemical kinetic model of vitrinite maturation and reflectances. Geochimica et Cosmochimica Acta 53, 2649-2657.

Burtner, R.L., Nigrini, A., Donelick, R.A., 1994. Thermochronoloy of Lower Cretaceous source rocks in the Idaho-Wyoming thrust belt. American Association Petroleum Geologists Bulletin 78, 1613 – 1636.

Chadouli, K., 2013. Caractérisation pétrographique appliquée à la modélisation pétrolière: Etudes de cas. PHD Thesis, Lorraine University, 244p.

Charriere, D., Pokryszka, Z., Belna, R., 2010. Effect of pressure and temperature in diffusion of CO_2 and CH_4 into coal from the Lorraine Basin (France). International Journal of Coal Geology 81, 373-380.

Courel, L., Liu, X.B., 1991. Variations in the geothermal history in coal basins ; relationship with basin dynamics. Bulletin de la Société géologique de France 162, 2, 363-370.

Donsimoni, M., 1981. Le bassin houiller lorrain, Synthèse géologique. Mémoire BRGM 117, 99 pp.

Durand, B., Alpern, B., Pittion, J.L., Pradier, B., 1986. Reflectance of vitrinite as a control of thermal history of sediments. In : Burrus, J. (Ed.), Thermal modelling in sedimentary basins. Editions Technip, pp. 441-474.

Duringer, P., Vecsei, A., 1998. Middle Triassic shallow-water limestones from the Upper Muschelkalk of estern France: the origin and depositional environment of some early Mesozoic fine-grained limestones. Sedimentary Geology 121, 57 – 70.

Durlet, C., Thierry, J., 2000. Modalités séquentielles de la transgression aalénobajocienne sur le sud-est du Bassin parisien. Bulletin de la Société géologique de France 171, 327 – 339.

Edel, J.-B., Schulmann, K., 2009. Geophysical constraints and model of the « Saxothuringian and Rheno-hercynian subduction-magmatic arc system» in NE France and SW Germany. Bulletin de la Société géologique de France 180, 545-558.

EGL (European Gas Limited), 2012. Une plateforme industrielle en Lorraine dédiée à la valorisation de champs gaziers stratégiques. Compte Rendu de la réunion à la région lorraine du 26 Juillet 2012.

Elixir petroleum limited, 2011. ASX announcement Moselle Permit, independent assessment of in-place volumes. Significant conventional and non-conventional hydrocarbon potential identified.

Espitalié, J., Laporte, J.L., Madec, M., Marquis, F., Leplat, P.M., Paulet, J., Boutefeu, A.P., 1977. Méthode rapide de caractérisation des roches mères, de leur potentiel pétrolier et de leur degré d'évolution. Revue de l'institut français du pétrole 32, 23-43.

Espitalié, J., Deroo, G., Marquis, F., 1985. La pyrolyse Rock-Eval et ses applications. Oil & Gas Science and Technology, Revue de l'institut français du pétrole 40, 5, 563-579.

Espitalié, J., Marqis, F., Sage, L., Barsony, I., 1987. Géochimie organique du Bassin de Paris. Oil & Gas Science and Technology, Revue de l'Institut Français du Pétrole 42, 3, 271-302.

Faure, J.L., Osadetz, K., Benaouali, Z.N., Schneider, F., Roure, F., 2004. Kinematic and petroleum modelling of the Alberta foothills and adjacent foreland, West of Calgary. Oil and Gas Science and Technology-Revue IFP 59, 81-108.

Fleck, S., 2001. Corrélation entre géochimie organique, sédimentologie et stratigraphie séquentielle pour la caractérisation des paléoenvironnements de dépôt. PhD Thesis, Université Henri Poincaré Nancy I, France, 387 pp.

Fleck, S., Michels, R., Izart, A., Elie, M., Landais, P., 2001. Paleoenvironmental assessment of Westphalian fluvio-lacustrine deposits of Lorraine (France) using a combination of organic geochemistry and sedimentology. International Journal of Coal Geology 48, 65-88.

Gallagher, K., Brown, R., Johnson, C., 1998. Fission Track Analysis and Its Applications to Geological Problems. Annual Review of Earth and Planetary Sciences 26, 519 – 572.

Garnier, Ch., Finqueneisel, G., Zimny, T., Pokryszka, Z., Lafortune, S., Defossez, P.D.C., Gaucher, E., 2011. Selection of coals of different maturities for CO_2 storage by modelling of CH_4 and CO_2 adsorption isotherms. International Journal of Coal Geology 87, 80-86.

Gaucher, E.C., Defossez, P.D.C., Bizi, M. Bonijoly, D., Disnar, J.-R., Laggoun-Defarge, E., Garnier, C., Finqueneisel, G., Zimny, J., Grgic, Pokryszka, S., Lafortune, S., Vidal Gibert S., 2011. Coal laboratory characterisation for CO_2 geological storage. Energy Procedia 4, 3147-3154.

Geologische Ubersichkarte von Saar (Geological map from Saar), 1979. Scale 1/200 000 Saarbrücken-Hannover CC 7102, Bundesrepublik Deutschland.

Green, P.F., Duddy, I.R., Gleadow, A.J.W., Tingate, P.R., Laslett, G.M., 1986. Thermal annealing of fission tracks in apatite : 1. A qualitative description. Chemical Geology 59, 237 – 253.

Green, P.F., Duddy, I.R., Laslett, G.M., Hegarty, K.A., Gleadow, A.J.W., Lovering, J.F., 1989. Thermal annealing of fission tracks in apatite : 4. Quantative modelling techniques and extension to geological timescales. Chemical Geology 79, 155 – 182.

Guillocheau, F., Robin, C., Allemand, P., Bourquin, S., Brault, N., Dromart, G., Friedenberg, R., Garcia, J.-P., Gaulier, J.- M., Gaumet, F., Grosdoy, B., Hanot, F., Le Strat, P., Mettraux, M., Nalpas, T., Prijac, C., Rigollet, C., Serrano, O., Grandjean, G., 2000. Meso-Cenozoic geodynamic evolution of the Paris Basin: 3D stratigraphic constraints. Geodinamica Acta 13, 189 – 246.

Henk, A., 1993. Late orogenic evolution in the Variscan Internides : the Saar-Nahe Basin, southwest Germany. Tectonophysics 223, 273-290.

Hertle, M., Littke, R., 2000. Coalification pattern and thermal modeling of the Permo-Carboniferous Saar Basin (SW-Germany). International Journal of Coal Geology 42, 273-296.

Hildenbrand, A., Kroos, B.M., Busch, A., Gaschnitz, R., 2006. Evolution of methane sorption capacity of coal seams as a function of burial history – A case study from the Campine basin (NE Belgium). International Journal of Coal Geology 66, 179-203.

Hurford, A.J., Green, P.F., 1983. The zeta age calibration of fission-track dating. Isotopic Geoscience 1, 285 – 317.

Hurford, A.J., 1990. Standardization of fission track dating calibration: Recommendation by the Fission Track Working Group of the I.U.G.S. Subcommission on Geochronology. Chemical Geology 80, 171 – 178.

International commission on Stratigraphy (ICS), 2014. Stratigraphic chart. http ://www.stratigraphy.org/ICSchart/Chronostrat2014-01.pdf

Izart, A., Vaslet, D., Briand, C., Broutin, J., Coquel, R., Davydov, V., Donsimoni, M., El Wartiti, M., Ensepbaev, T., Geluk, M., Goreva, N., Görür, N., Iqbal, N., Joltaev, G., Kossovaya, O., Krainer, K., Laveine, J.-P., Makhlina, M., Maslo, A., Nemirovskaya, T., Kora, M., Kozitskaya, R., Massa, D., Mercier, D., Monod, O., Oplustil, S., Schneider, J., Schönlaub, H.,Stschegolev, A., Süss, P., Vachard, D., Vai, G.B., Vozarova, A., Weissbrod, T., Zdanowski, A., 1998. Stratigraphic correlations between the continental and marine Tethyan and Peri-Tethyan basins during the Late Carboniferous and the Early Permian. In: Crasquin-Soleau, S., Izart, A., Vaslet, D., De Wever, P. (Eds.), Peri-Tethys: stratigraphic correlations 2. Geodiversitas 20, 4, pp. 521-595.

Izart, A., Stephenson, R., Vai, G.B., Vachard, D., Le Nindre, Y., Vaslet, D., Fauvel, P.-J., Süss, P., Kossovaya, O., Chen, Z., Maslo, A., Stovba, S., 2003. Sequence stratigraphy and Correlation of the Late Carboniferous and Permian in CIS, Europe, Tethyan area, North Africa, China, Gondwanaland and USA. Palaeogeography, Palaeoclimatology, Palaeoecology 196, 59-84.

Izart, A., Palain, C., Malartre, F., Fleck, S. Michels, R., 2005. Palaeoenvironments, paleoclimates and sequences of Westphalian deposits of Lorraine coal Basin (Upper Carboniferous, NE France). Bulletin de la Société géologique de France 176, 3, 301-315.

Juch, D., Gaschnitz, R., Thieleman, T., 2004. The influence of geological history on coal mine gas distribution in the Ruhr district – a challenge for future research and recovery. Geologica Belgica 7/3-4, 191-199.

Kelch, H.-J., Reible, P., 1976. Beschreibung der spülproben und kerne der Bohrung Saar 1. Geologisches Jahrbuch A27, 29-89.

Ketcham, R.A., Donelick, R.A., Carlson, W. D., 1999. Variability of apatite fission-track annealing kinetics: III. Extrapolation to geological time scales. American Mineralogist 84, 1235 – 1255.

Ketcham, R.A., Donelick, R.A, Donelick, M.B., 2000. AFTSolve: A program for multi-kinetic modeling of apatite fission-track data. Geological Materials Research 2, 1 – 32.

Ketcham R.A., Carter A., Donelick R.A., Barbarand J., Hurford A.J., 2007. Improved modeling of fission-track annealing in apatite. American Mineralogist 92, 799 – 810.

Ketcham, R.A., 2005. Forward and inverse modeling of low-temperature thermochronometry data. Review in Mineralogy and Geochemistry 58, 275 – 314.

Korsch, R.J., Schäffer, A., 1995. The Permo-Carboniferous Saar-Nahe Basin, south-west Germany and north-east France : basin formation and deformation in a strike-slip regime. Geologische Rundschau 84, 293-318.

Lampe, C., Person, M., 2002. Advective cooling within sedimentary rift basins : application to the Upper Rhine Graben (Germany). Marine and Petroleum Geology 19, 361-375.

Laslett, G.M., Green, P.F., Duddy, I.R., Gleadow, A.J.W., 1987. Thermal annealing of fission

tracks in apatite : 2. A quantative analysis. Chemical Geology 65, 1 – 13.

Laveine, J.P., 1974. Précisions sur la répartition stratigraphique des principales espèces végétales du Carbonifère supérieur de Lorraine. C.R. Acad. Sci. Fr., 278, (D), 851-854.

Le Roux, J., 1980. La tectonique de l'auréole orientale du Bassin de Paris. Ses relations avec la sédimentation. Bulletin de la Société géologique de France 4, 655-662.

Le Roux, J., 2000. Structuration du Nord-Est du bassin de Paris. Bulletin d'Information des géologues du Bassin de Paris 37, 4, 13-34.

Le Roux, J., Harmand, D., 2003. Origin of the hydrographic network in the Eastern Paris Basin and its border massifs. Hypothesis, structural, morphologic and hydrographic consequences. Géologie de la France 1, 105-110.

Le Solleuz, A., Doin, M.P., Robin, C., Guillocheau, F., 2004. From a mountain belt collapse to a sedimentary basin development. 2-D thermal model based on inversion of stratigraphic data in the Paris Basin. Tectonophysics 386, 1-27.

Littke, R., Büker, C., Hertle, M., Karg, H., Stroetmann-Heinen, V., Oncken, O., 2000. Heat flow evolution, subsidence and erosion in the Rheno-Hercynian orogenic wedge of central Europe. Geological Society London Special Publications 179, 231-255.

Lucazeau, F., Vasseur, G., 1989. Heat flow density data from France and surrounding margins. Tectonophysics 164, 251-258.

Mazumber, S., Wolf, K.-H.A.A., Elevaut, K., Ephraim, R., 2006. Application of X-ray computed tomography for analyzing cleat spacing and cleat aperture in coal samples. Internation Journal of Coal Geology 68, 205-222.

Mégnien, C., 1980. Tectogenèse du Bassin de Paris : étapes de l'évolution du bassin. Bulletin de la Société géologique de France 4, 669 – 680.

Mégnien, C., Mégnien, F., Debrand-Passard, S., 1980. Synthèse Géologique du Bassin de Paris. Mémoires du B.R.G.M., 101, 102, 103, Orléans, 460 pp.

Menetrier, C., 2005. Modélisation thermique appliquée aux bassins sédimentaires: Bassin de Paris (France) et Bassin de Sabinas (Mexique). PhD Thesis, Université Henri Poincaré Nancy I, France, 274 pp.

Menetrier, C., Elie, M., Martinez, L., Le Solleuz, A., Disnar, J.R., Robin, C., Guillocheau, F., Rigollet, C., 2005. Estimation of the maximal burial paleotemperature for Toarcian and Callovo-Oxfordian samples in the central part of the Paris Basin using organic markers. Compte Rendu Geosciences 337, 15, 1323-1330.

Milton-Worssell, R., Smith, K., Mc Grandle, A., Watson, J., Cameron, D., 2010. The search for a Carboniferous petroleum system beneath the Central North Sea. In : Vining, B.A., Pickering, S.C. (Eds.), Petroleum Geology : From mature basin to new fronteer. Proceeding of the 7th Petroleum Geology Conference. The Geological Society of London, 57-75.

Perrodon, A., Zabek, J., 1991. Paris Basin, (interior intracratonic basins). American Association of Petroleum Geologists Memoir 51, 633 – 679.

Poulet, M., Espitalié, J., 1987. Hydrocarbon migration in the Paris Basin. In: Doligez, B. (Ed.), Migration of hydrocarbons in sedimentary basins. 2d IFP Exploration Research Conference, Paris, 1987, Editions Technip, 131-171.

Prijac, C., Doin, M.P., Gaulier, J.M., Gillocheau, F., 2000. Subsidence of the Paris Basin and its bearing on the late variscan lithosphere evolution: a comparison between Plate and Chablis models. Tectonophysics 323, 1-38.

Privalov, V.A., 1991. A new method to determine geological structure hierarchy. Journal of Changchun university (China) 4, 397-402.

Pruvost, P., 1934. Bassin houiller de la Sarre et de la Lorraine, t. III : Descrption géologique. Etudes gîtes minéraux, France, Lille, Imprimerie Danel.

Quesnel, F., 2003. Paleoweathering and paleosurfaces from northern and eastern France to belgium and Luxembourg : geometry, dating and geodynamic implications. Géologie de la France 1, 95-104.

Rodriguez, C.F., Laiginhas, C., Fernandes, M., Lemos de Sousa, M.J., Dinis, M.A.P., 2014. The coal cleat system : A new approach to its study. Journal of Rock Mechanics and Geotechnical Engineering 6, 208-218.

Roscher, M., Schneider, J.W., 2006. Permocarboniferous climate: Early Pennsylvanian to Late Permian climate development of central Europe in a regional and global context. In: Lucas, S.G., Cassini, G., Schneider, J.W. (Eds.), Non Marine Permian Chronology and Correlation. The Geological Society of London 265, 95-136.

Schäfer, F., Oncken, O., Kemnitz, H., Tomer, R., 2000. Upper-plate deformation during collisional orogeny: a case study from the German Variscides. In: Franke, W., Haak, V., Oncken, O., Tanner, D. (Eds), Orogenic processes: Quantification and Modelling in the Variscan belt. Geological Society, London, Special Publications 179, 281-302.

Schneider, J.W., Roscher, M., 2010. The Late Variscan molasses (Late Carboniferous to Late Permian) from the Saxo-Thuringian zone. In : Linnemann, U., Romer, R.L. (Eds.), Pre-Mesozoic geology of Saxo-Thuringia – From the Cadomian active margin to the Variscan orogen. Schweizerbart, Stuttgart, 323-346.

Sclater, J.-G., Christie, P.-A.F., 1980. Continental streching : an explanation od the post-Mid-Cretaceous subsidence of the central North Sea Basin. Journal of Geophysical Research 85, 3711-3739.

Sweeney, J.J., Burnham, A.K., 1990.Evaluation of a simple model of vitrinite reflectance based on chemical kinetics. The American Association of Petroleum Geologists Bulletin 74, 10, 1559-1570.

Teichmüller, M., Teichmüller, R., 1971. Das Rhein-Ruhr-Ravier Inkohlung. Fortschrift Geology Rheinland Westfalen 19, 47-56.

Theveniaut, H., Quesnel, F., Wyns, G., Hugues, G., 2007. Palaeomagnetic dating of the « Borne de Fer » ferricrete (NE France) : Lower Cretaceous continental weathering. Palaeogeography, Palaeoclimatology, Palaeoecology 253, 271-279.

Ungerer, P., Espitalié, J., Marquis, F., Durand, B., 1986. Use of kinetic models of organic matter evolution for the reconstruction of paleotemperatures. Application to the case of the Gironville well (France). In : Burrus, J. (Ed.), Thermal modelling in sedimentary basins. Editions Technip, pp. 531-546.

Von Seckendorff, V., Arz, C., Lorenz., V., 2004. Magmatism of the late variscan intermontane Saar-Nahe Basin (Germany) : a review. Geological Society, London, Special Publications 223, 361-391.

Wygrala, B.P., 1988. Integrated computer-aided basin modeling applied to analysis of hydrocarbon generation history in a northern Italian oilfield. Organic Geochemistry 13, 187-197.

Ziegler, P.A., 1990. Geological Atlas of Western and Central Europe. Shell International Petroleum Meeting, The Hague. Distributed by Geological Society Publication House, Bath, 239 pp.

List of Figures and Tables

Fig. 7: Fission tracks from Triassic sandstones in the Rn 8 borehole

A: Radial plot representation of the apatite fission track-data for a sample at 585m deep

B: Track-length frequency

C: Thermal history modelling of the apatite fission-track data. Results in the temperature-time diagram are indicated by two colors indicating matching between data and model: purple envelopes indicate a good match (fit>0.5 estimated using Kolmogorov-Smirnov test and Kuiper's Statistic) and green envelopes indicate acceptable fit (between 0.05 and 0.5).

Fig. 8: 1D modelling from the Rn 8 borehole

A: erosion of Jurassic and Triassic after the Cretaceous and B: erosion of Late Jurassic before the Cretaceous and Mid-Jurassic, Early Jurassic and Triassic after the Cretaceous, CET: Cretaceous erosion thickness and HF: Heat flow.

Fig. 9: Calibration of the 1D modelling with vitrinite reflectances (VR)

CET: Cretaceous erosion thickness, HF: Heat flow (50 mW/m2 (W)-60 (SP-Tr)-40 (Te-R)

for all boreholes, except 400 mW/m2 during Permian for Chevraumont borehole),

PET: Paleozoic erosion thickness, WB: Westphalian B and WAN: Westphalian A-Namurian.

Fig. 10: Calibration for diverse HF and ET from Gironville borehole 1D and extracted from 2D modelling of Toul 08 seismic line

CET: Cretaceous erosion thickness, HF: Heat flow, MET: Mesozoic erosion thickness,

PET: Paleozoic erosion thickness, SP: Stephanian-Permian, Te-R: Tertiary to Recent, Tr: Triassic, W: Westphalian.

Fig. 11: Maximal paleotemperatures at the top of Cretaceous in the EPLY 02-LOR 09 and TOUL 08 seismic lines

Bunt : Buntsandstein, JCR : Jurassic and Cretaceous, Perm : Permian, Ste : Stephanian and WB, C and D : Westphalian B, C and D.

Fig. 12: Burial and temperature history in Gironville, Saulcy and Vaxy boreholes

Fig. 13: Hydrocarbon maturity in the EPLY 02-LOR 09 and TOUL 08 seismic lines with kinetics of type III

Bunt : Buntsandstein, Perm : Permian, Ste : Stephanian and WB, C and D : Westphalian B, C and D.

Fig. 14: Oil and gas generation (Mtons/km^3) in the EPLY 02-LOR 09 seismic line

Bunt : Buntsandstein, Perm : Permian, Ste : Stephanian and WB, C and D : Westphalian B, C and D.

Fig. 15: Oil and gas generation (Mtons/km^3) in the TOUL 08 seismic line

Fig. 16: Methane adsorption in coal seams (m^3/ton coal) vs. VR (%) after Garnier et al. (2011) in A and Hildenbrand et al. (2006) in B, and methane adsorption (m^3/ton coal) in Gironville (B), Saulcy (C) and Faulquemont (D) boreholes after our VR curves modelled by Petromod

Fig. 17: Application of tomography for analyzing cleat system in a coal sample from coal seam 10 (1239m depth) in the Westphalian D of the Tritteling 1 borehole.

A : Direction of diaclases in yellow in the coal seams 6, 8 and 9 after underground mapping in coal mine Faulquemont after Bles and Lozes (1980) ; B : Face and Butt cleats in the coal sample from Tritteling 1.

Fig. 18: Application of tomography for analyzing cleat spacing (A), aperture (B) and connectivity (C) in a coal sample from coal seam 10 (1239m depth) in the Westphalian D of the Tritteling 1 borehole.

Fig. 19: Gas (red) migration pathways in the EPLY 02- LOR 09 and Toul 08 sections

Bunt : Buntsandstein, Perm : Permian, Ste : Stephanian and WB, C and D : Westphalian B, C and D.

Table 1: Location of boreholes

X and Y coordinates are from Lambert 1 grid reference.

Table 2 : Thermal conductivity (at temperature=20°C), heat capacity (at temperature=20°C) and density of pure lithology

Table 3: Input data for the Gironville 001 borehole

An: anhydrite, Ch: chalk, Cl: claystone, Co: Conglomerate, Do: dolomite, Gr: limestone (grainstone), Ha: halite, HF: heat flow, HI: hydrogen index, OM: organic matter, Ma: marl, Mu: limestone (mudstone), P: petroleum data, RE: reservoir rock, Sa: sandstone, SE: seal rock, SR: source rock, TOC: total organic carbon, VR: vitrinite reflectance.

Table 4: Present and eroded thickness (Thick) of formations in boreholes

Table 5: Permian and Carboniferous Facies

Cl: claystone, Co: conglomerate and Sa: sandstone.

Table 6: OM and petroleum data and Heat Flows

HF: heat flow, HI: hydrogen index, OM: organic matter, P: petroleum data, RE: reservoir rock, SE: seal rock, SR: source rock, TOC: total organic carbon, VR: vitrinite reflectance.

Table 7: Heat flow, Erosion thickness, Oil and gas windows and OM transformation rates (TR)

C: Cretaceous, Extr.: 1D extraction from 2D, M: Mesozoic, P: Paleozoic, SP: Stephanian and Permian, ST: Stephanian, T: total, TR: OM transformation rates, Tr: Triassic, Te-R: Tertiary to Recent, W: Westphalian, WA, B, C and D: Westphalian A, B, C and D.

Table 8: Expulsion time, and oil and gas generation and storage

Extr.: 1D extraction from 2D, ST: Stephanian, WA, B, C and D: Westphalian A, B, C and D.

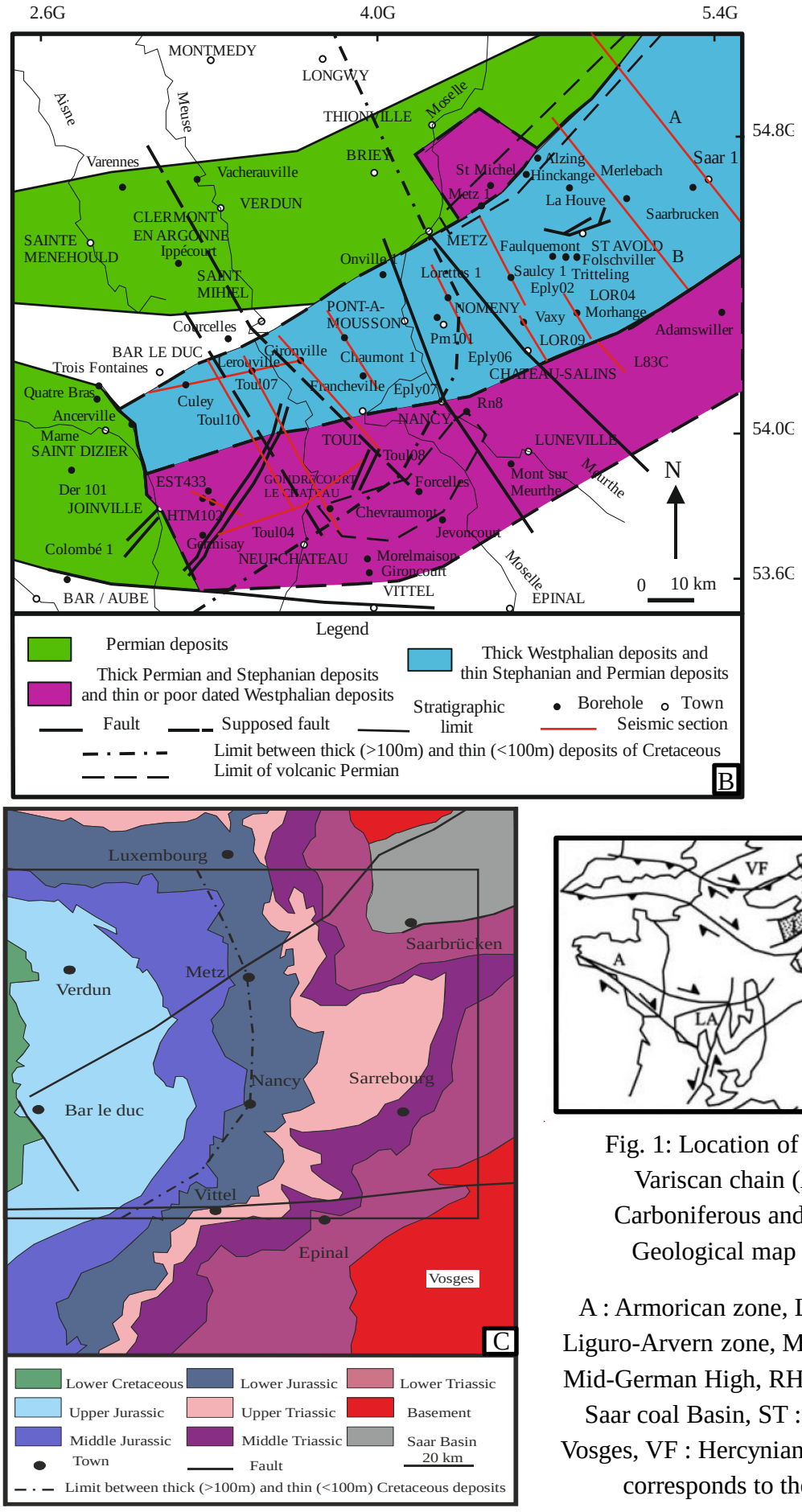

Fig. 1: Location of the Lorraine Basin in the Variscan chain (A), Geological map of Carboniferous and Permian basins (B) and Geological map of Mesozoic cover (C)

A : Armorican zone, L : Lorraine coal Basin, LA : Liguro-Arvern zone, M : Moldanubian zone, MGH : Mid-German High, RH : Rheno-Hercynian zone, S : Saar coal Basin, ST : Saxo-Thuringian zone, V : Vosges, VF : Hercynian foredeep. The rectangle in C corresponds to the contour of the map B.

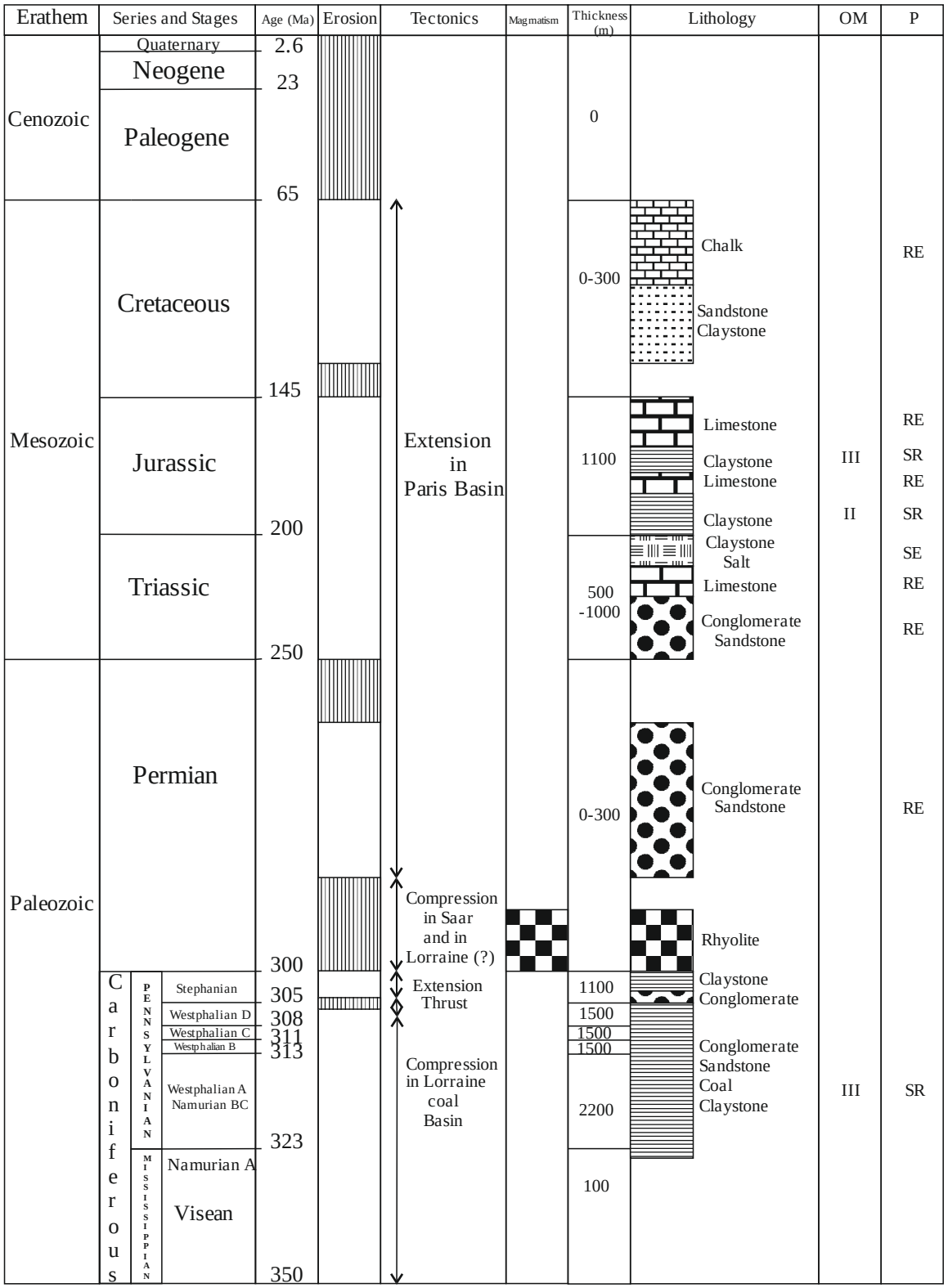

Fig. 2: Chrono- and lithostratigraphy from the Lorraine
Major erosional, magmatic and tectonic events are shown.
OM: Organic matter type, P: Petroleum type, RE: reservoir rock, SE: seal rock, SR: source rock.

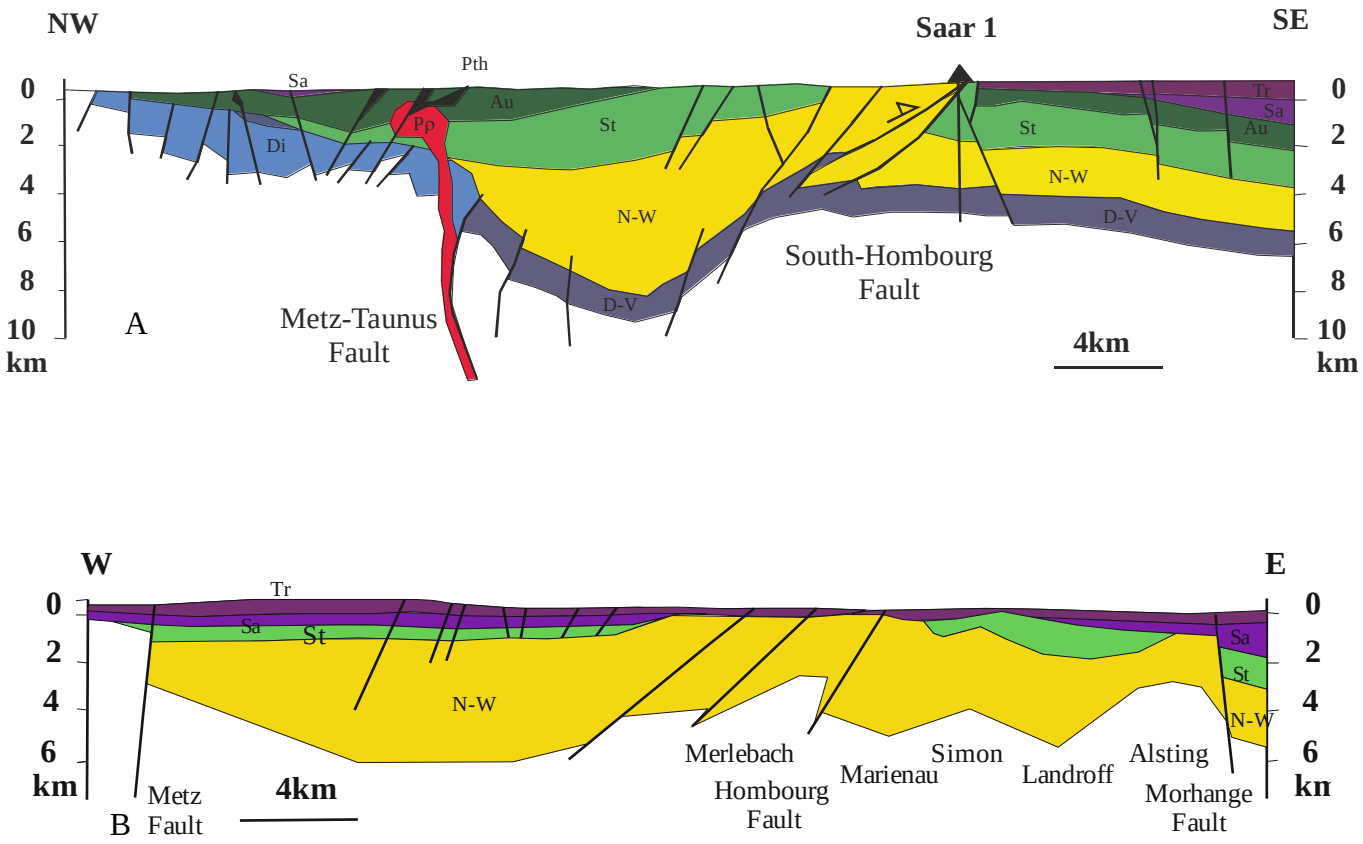

Fig. 3: Geological cross-sections from the Saar (A) and Lorraine (B) coal basins

Au : Autunian, D-V : Middle and Late Devonian and Early Carboniferous, Di : Early Devonian, N-W : Namurian and Westphalian, Pth : Permian tholeite, Pr : Permian rhyolite, Sa : Saxonian, Saar 1: Saar 1 borehole, St : Stephanian, Tr : Triassic.

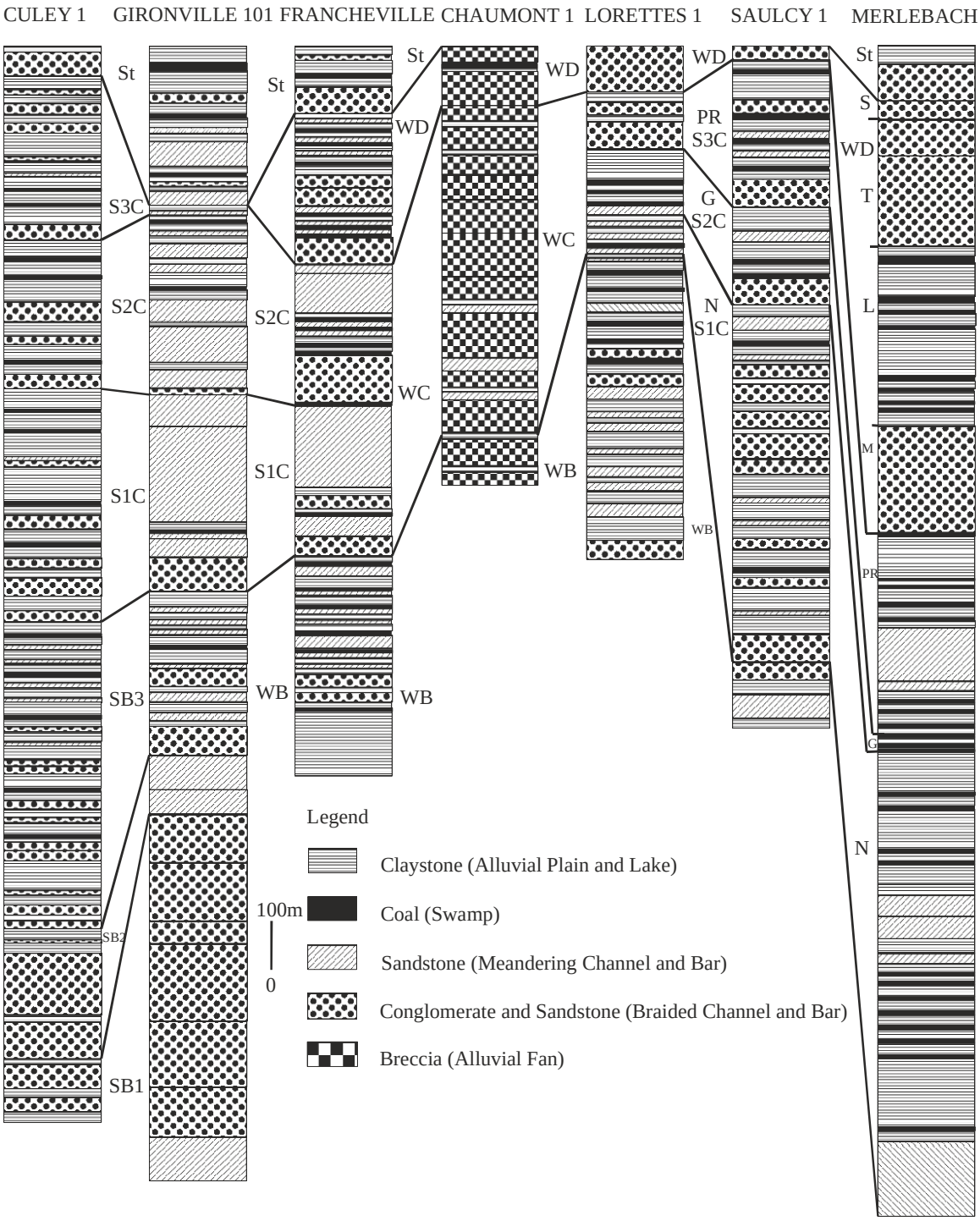

Fig. 4 : Stratigraphic columns of the Carboniferous from the Lorraine coal Basin

G : Geisheck Formation, L : Laudrefang Formation, M : Conglomérat de Merlebach Formation, N : Neunkirchen Formation, PR : Petite Rosselle Formation, SB1 to SB3 and SC1 to SC3 : Third order sequences from the Westphalian B and C, S : Steinbesch Formation, St : Stephanian composed of the Holz conglomerate Formation, T : Tritteling Formation, WB : Westphalian B, WC : Westphalian C, WD : Westphalian D.

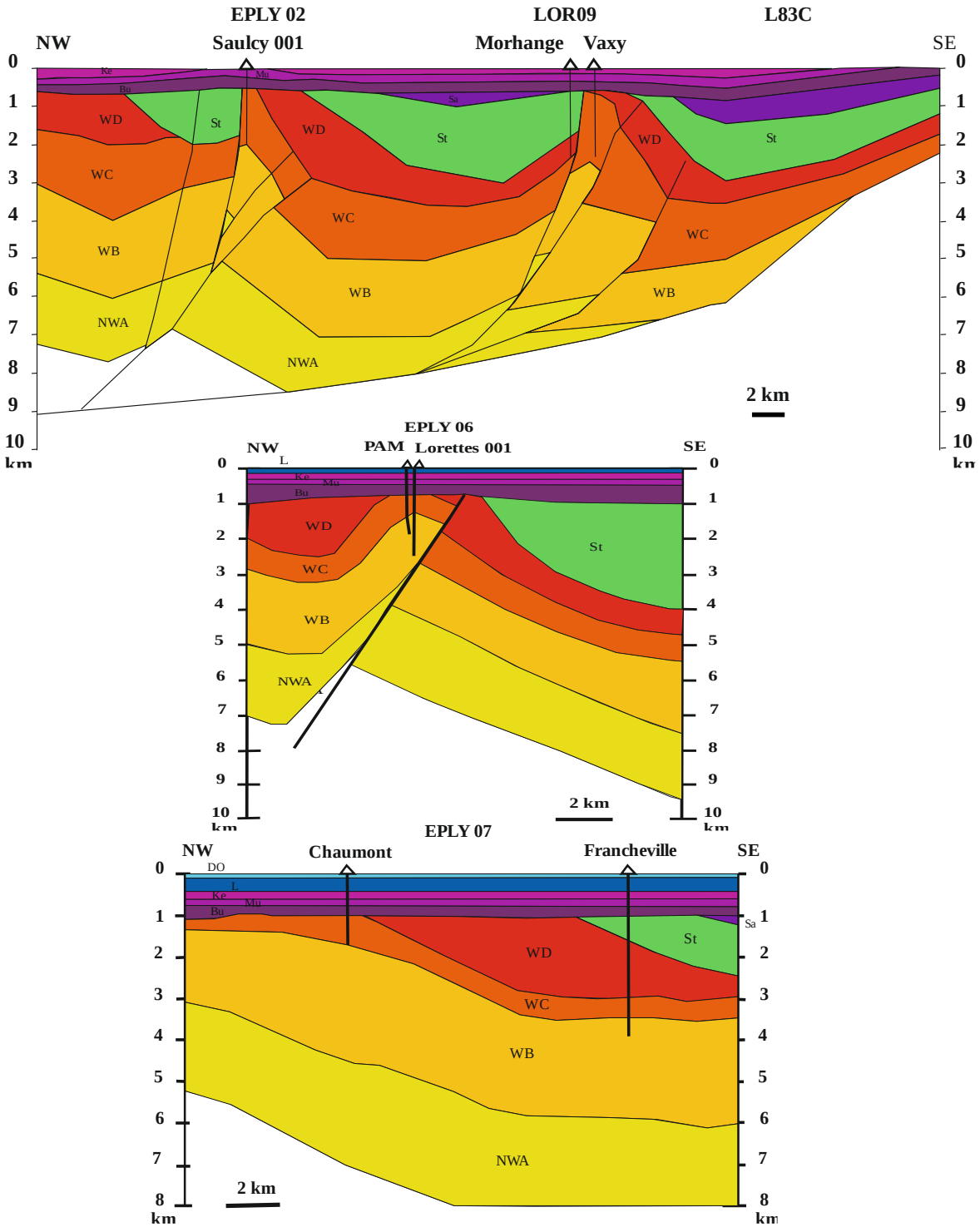

Fig. 5: Geological cross-sections based on the EPLY 02-LOR 09-L83C, EPLY 06 and EPLY 07 seismic sections

Ba : Bajocian and Bathonian, Bu : Buntsandstein, COA : Callovian and Oxfordian Claystone, Do : Dogger, L : Liassic, Mu : Muschelkalk, N-WA : Namurian and Westphalian A, Ke : Keuper, OC : Limestone of Oxfordian, Sa : Saxonian, St : Stephanian, WB : Westphalian B, WC : Westphalian C, WD : Westphalian D.

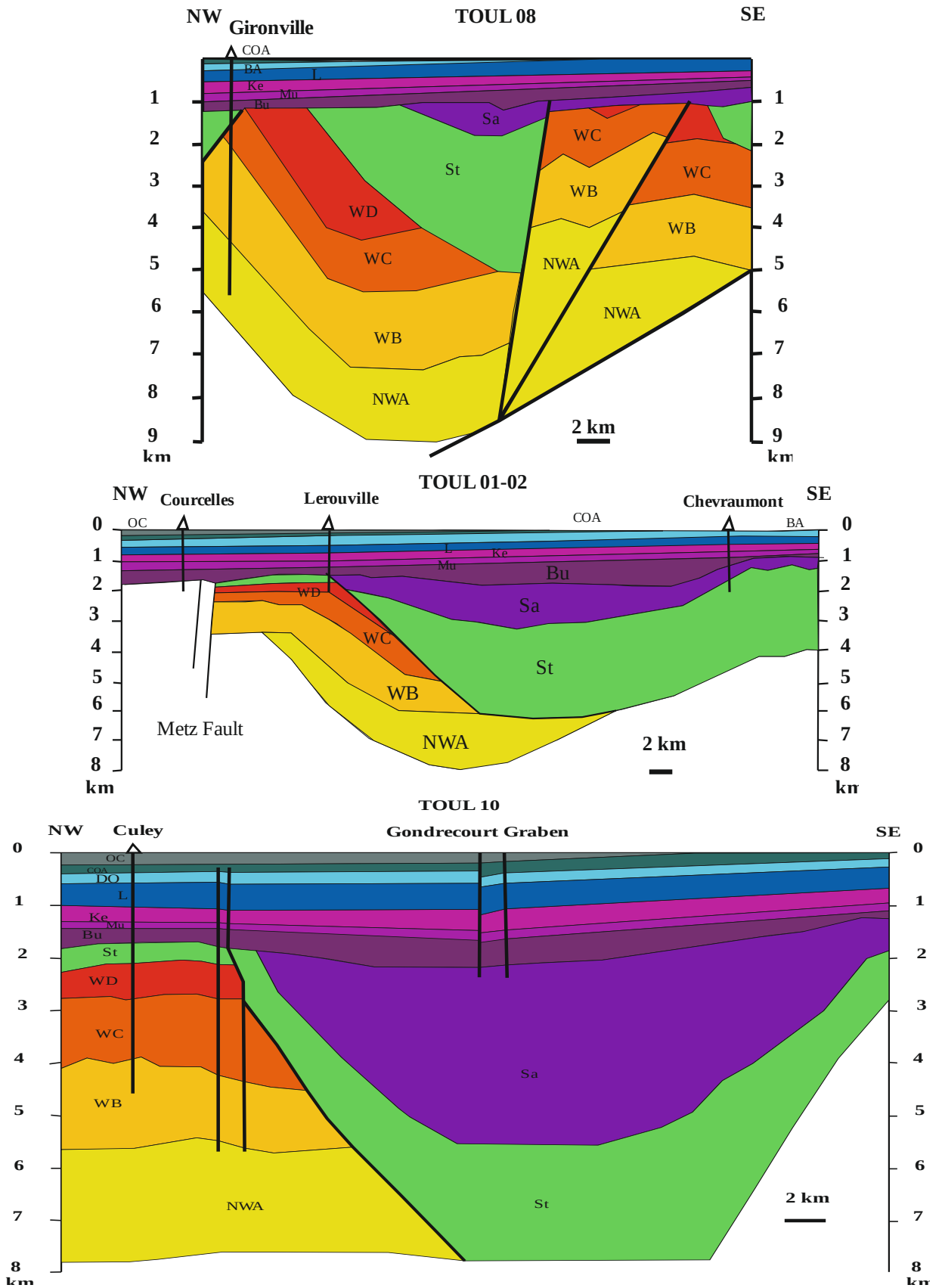

Fig. 6: Geological cross-sections based on the TOUL 08, TOUL 01-02 and TOUL 10 seismic sections. Bu : Buntsandstein, Do : Dogger, L : Liassic, Mu : Muschelkalk, N-WA : Namurian and Westphalian A, Ke : Keuper, Sa : Saxonian, St : Stephanian, WB : Westphalian B, WC : Westphalian C, WD : Westphalian D.

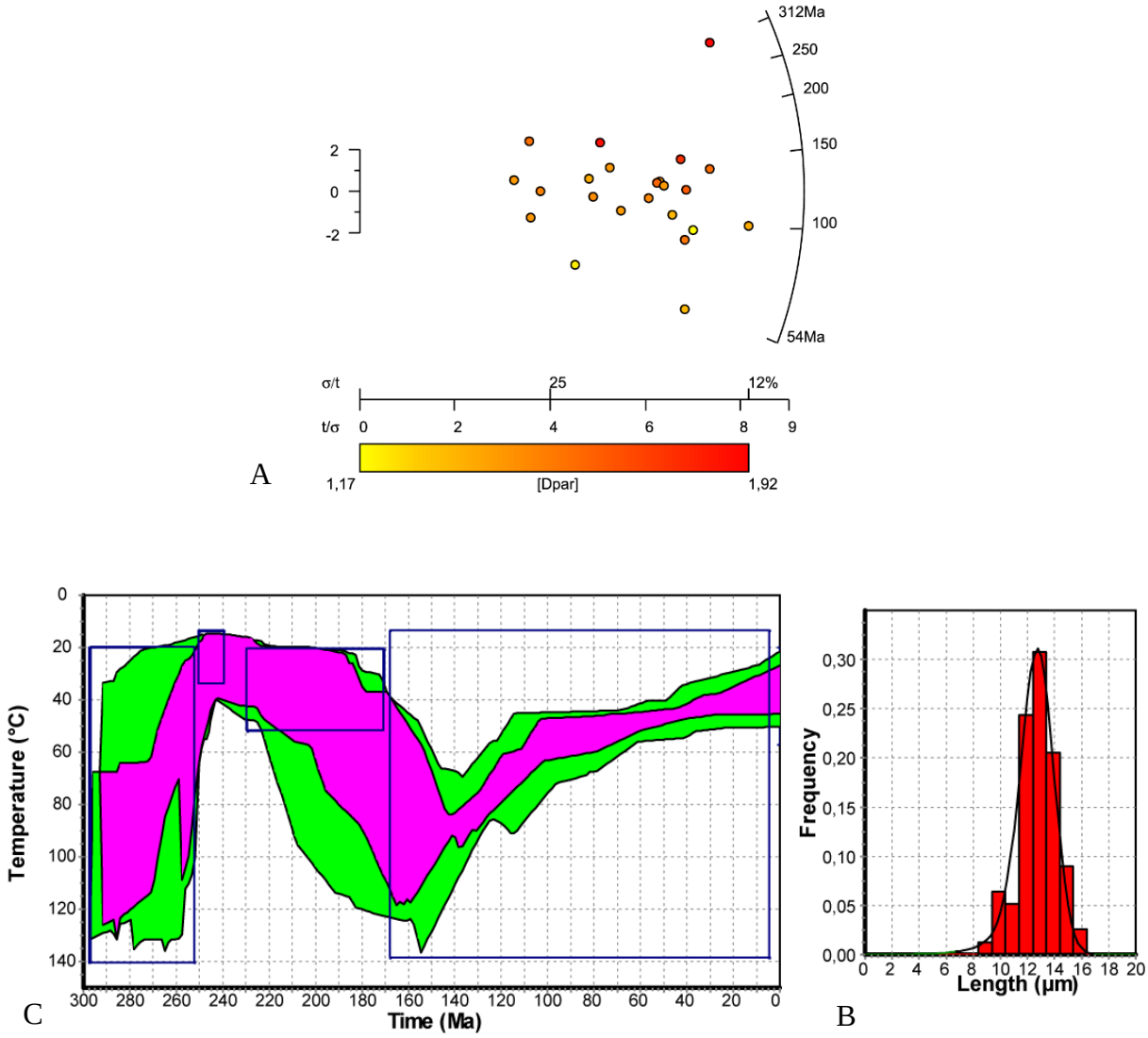

Figure 7: Fission tracks from Triassic sandstones in the Rn 8 borehole

A: Radial plot representation of the apatite fission track-data for a sample at 585m deep

B: Track-length frequency

C: Thermal history modelling of the apatite fission-track data. Results in the temperature-time diagram are indicated by two colors indicating matching between data and model: purple envelopes indicate a good match (fit>0.5 estimated using Kolmogorov-Smirnov test and Kuiper's Statistic) and green envelopes indicate acceptable fit (between 0.05 and 0.5).

Burial and temperature history

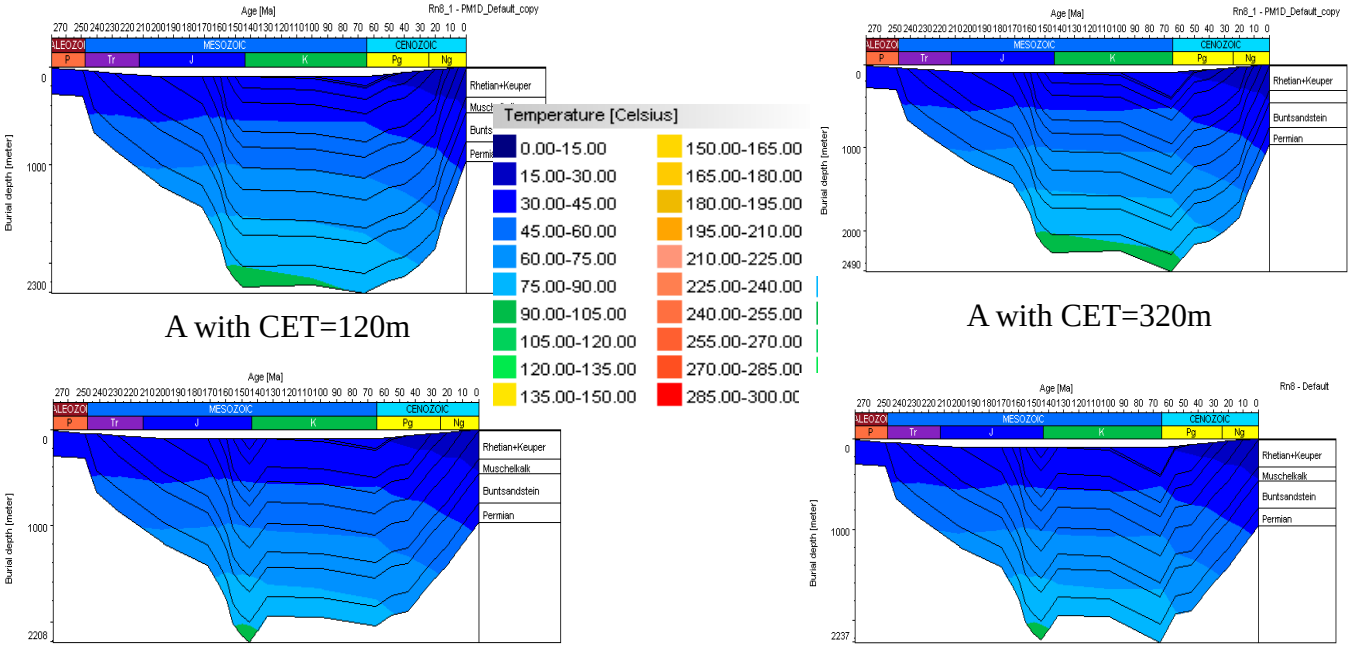

A with CET=120m

A with CET=320m

B with CET=120m

B with CET=320m

Calibration for A (left) and B (right)

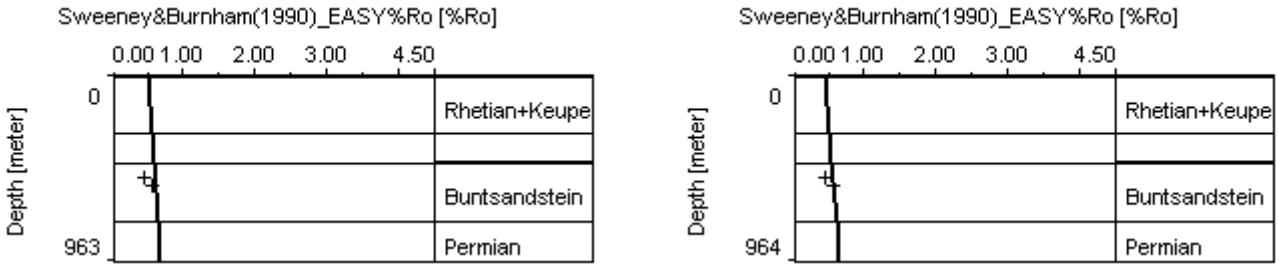

HF= from 60 (Permian) to 50 (Recent) mW/m^2
and CET=120m and 320m

Fig. 8: 1D modelling from the Rn 8 borehole
A: erosion of Jurassic and Triassic after the Cretaceous and B: erosion of Late Jurassic before the Cretaceous and Mid-Jurassic, Early Jurassic and Triassic after the Cretaceous ,
CET: Cretaceous erosion thickness and HF: Heat flow.

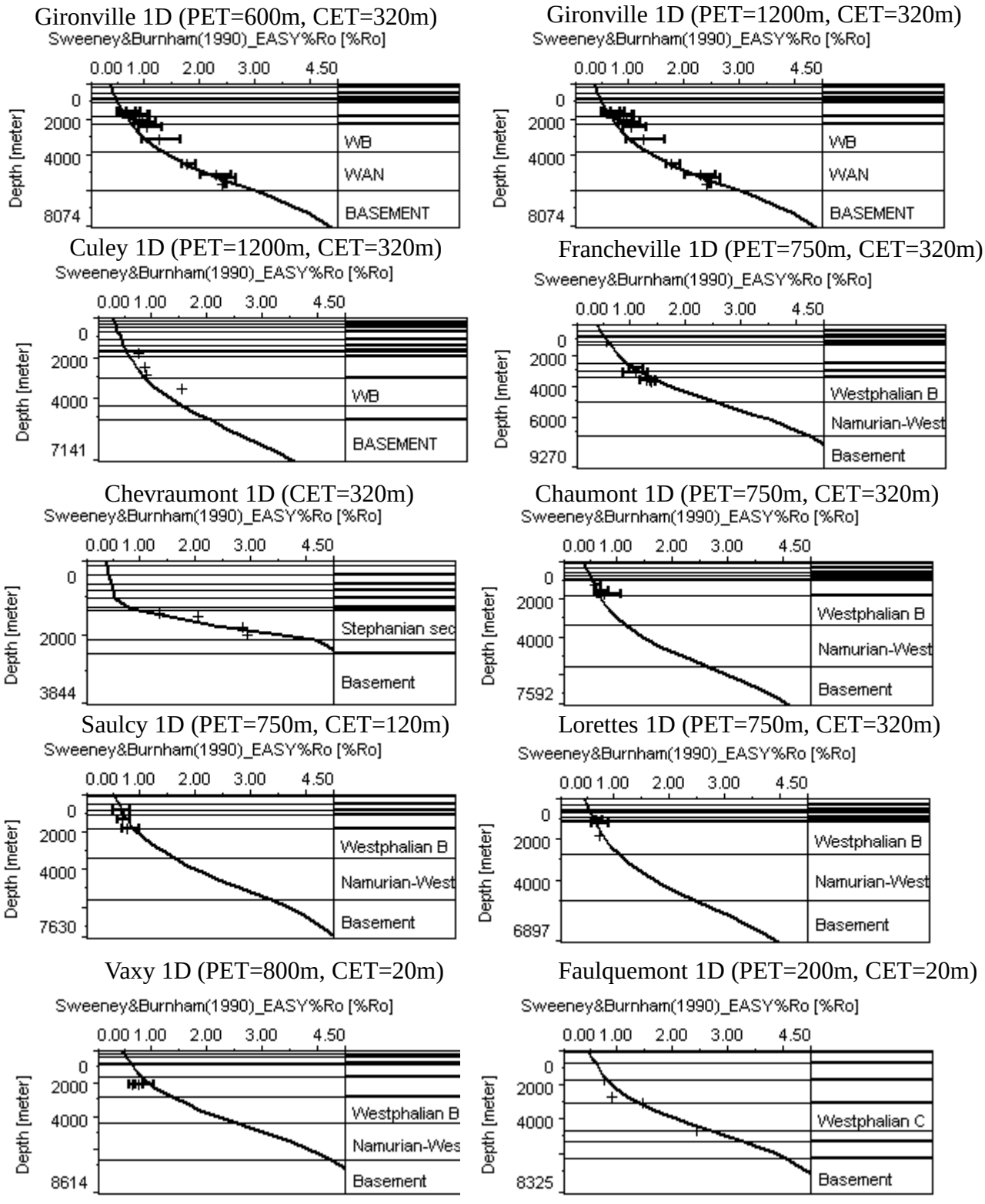

Fig. 9: Calibration of the 1D modelling with vitrinite reflectances (VR)
CET: Cretaceous erosion thickness, HF: Heat flow (50 mW/m^2 (W)-60 (SP-Tr)-40 (Te-R) for all boreholes, except 400 mW/m^2 during Permian for Chevraumont borehole),
PET: Paleozoic erosion thickness, WB: Westphalian B and WAN: Westphalian A-Namurian.

Gironville 1D (PET=1200m and CET=320m)

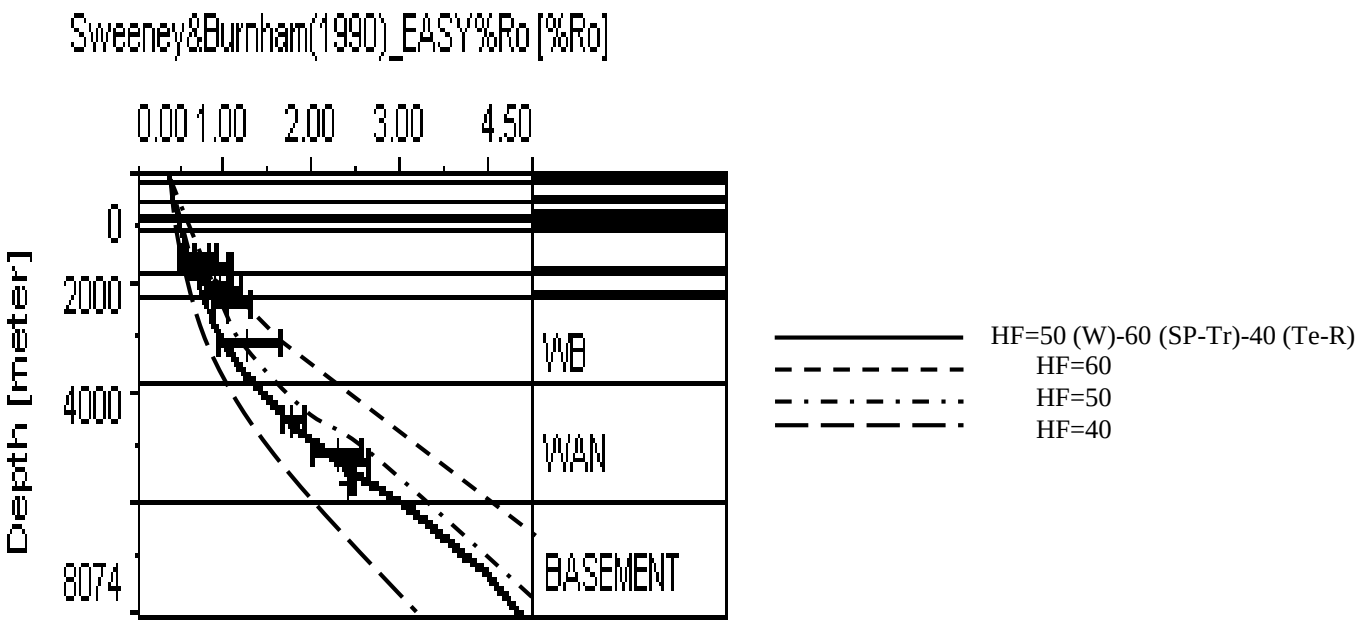

Gironville extracted from Toul 08

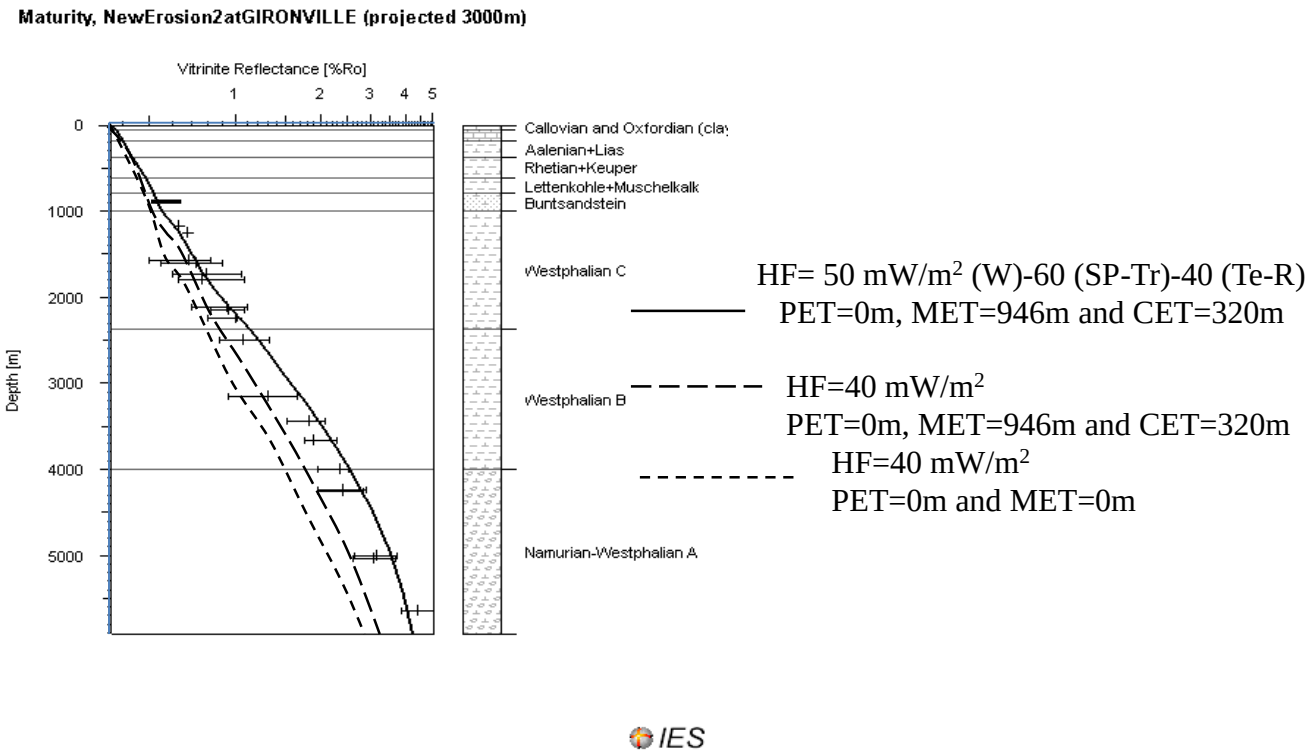

Fig. 10: Calibration for diverse HF and ET from Gironville borehole 1D and extracted from 2D modelling of Toul 08 seismic line

CET: Cretaceous erosion thickness, HF: Heat flow, MET: Mesozoic erosion thickness, PET: Paleozoic erosion thickness, SP: Stephanian-Permian, Te-R: Tertiary to Recent, Tr: Triassic, W: Westphalian.

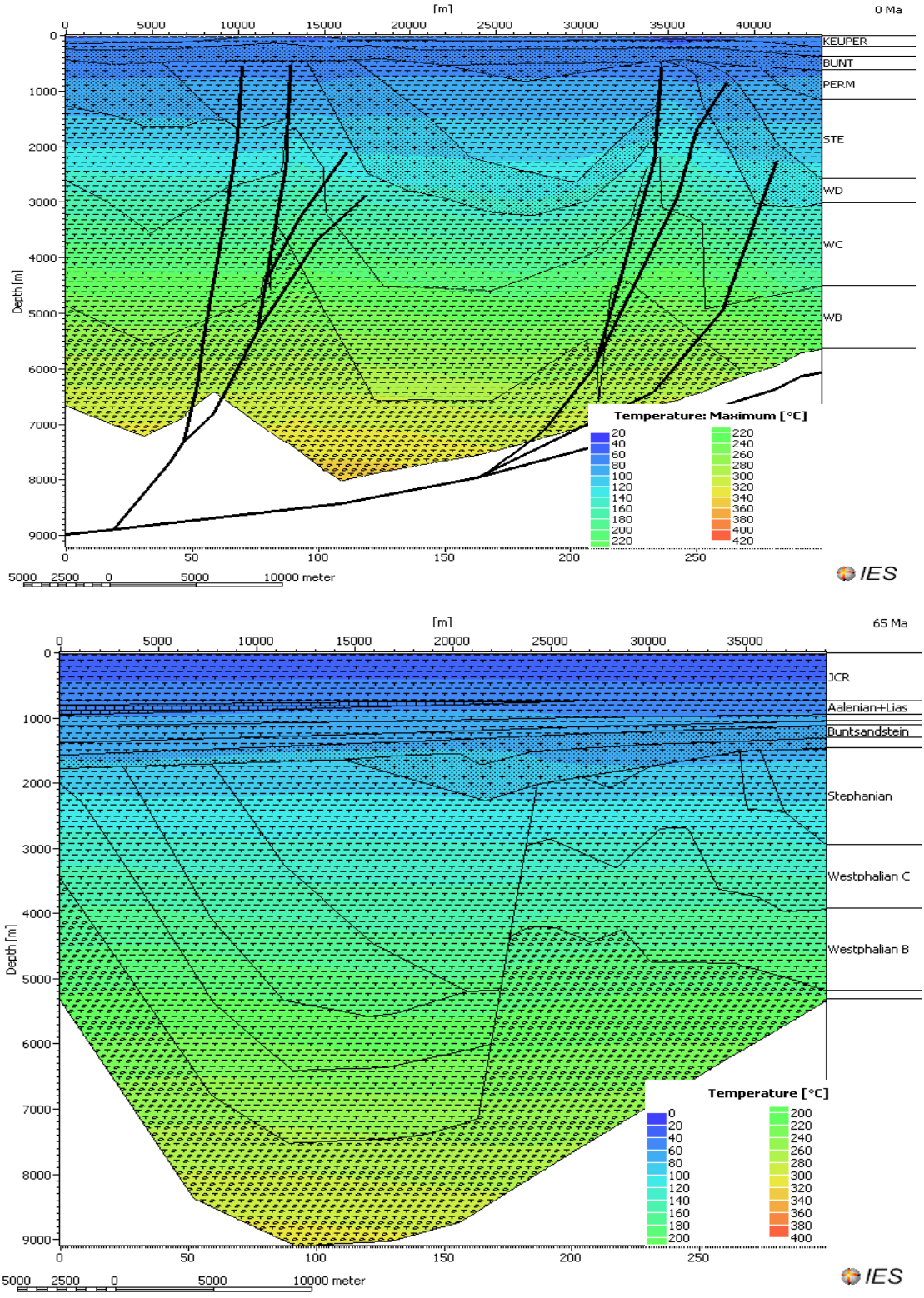

Fig. 11: Maximal paleotemperatures in the EPLY 02-LOR 09 and TOUL 08 seismic lines Bunt : Buntsandstein, JCR : Jurassic and Cretaceous, Perm : Permian, Ste : Stephanian and WB, C and D : Westphalian B, C and D.

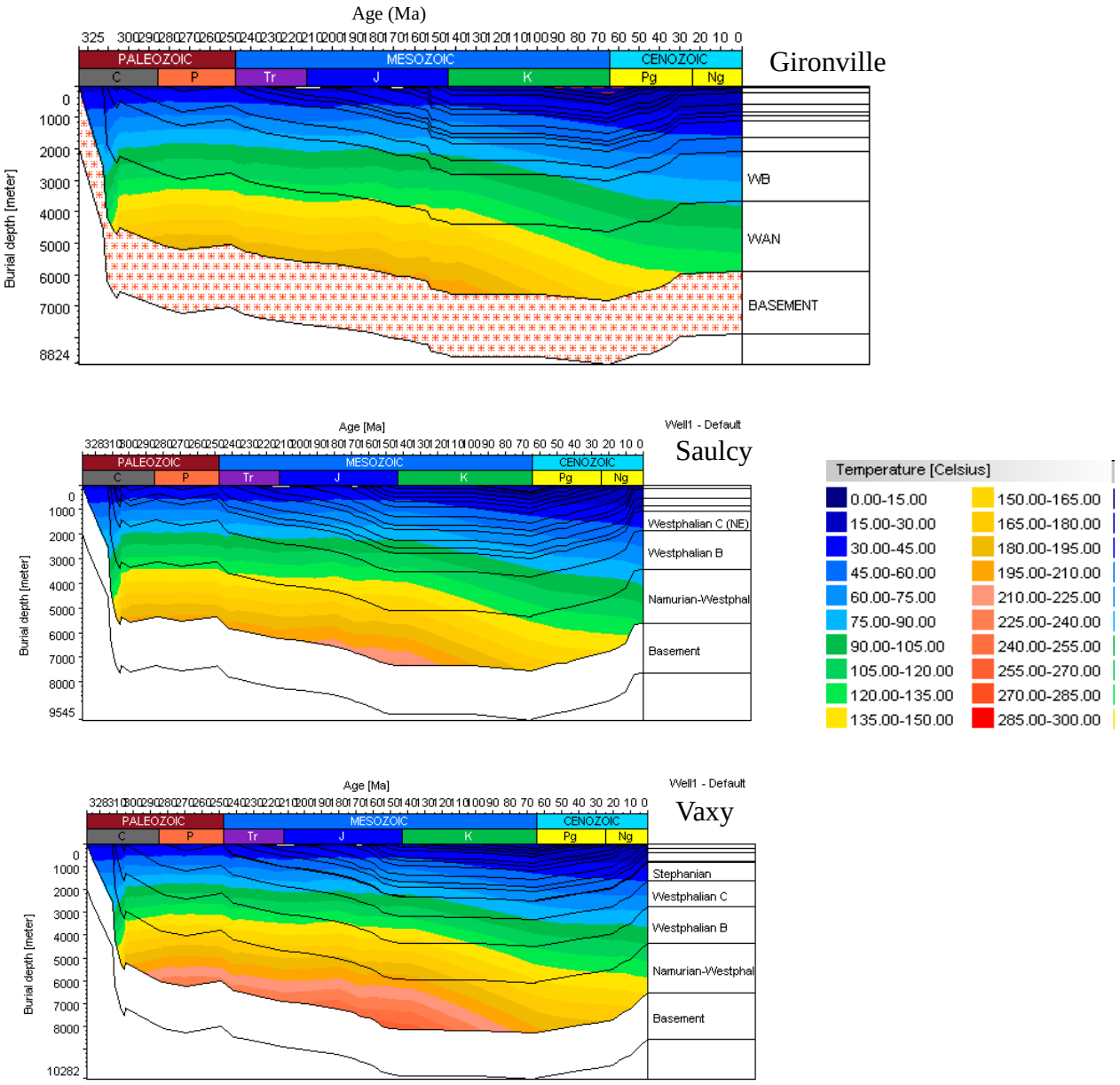

Fig. 12: Burial and temperature history in Gironville, Saulcy and Vaxy

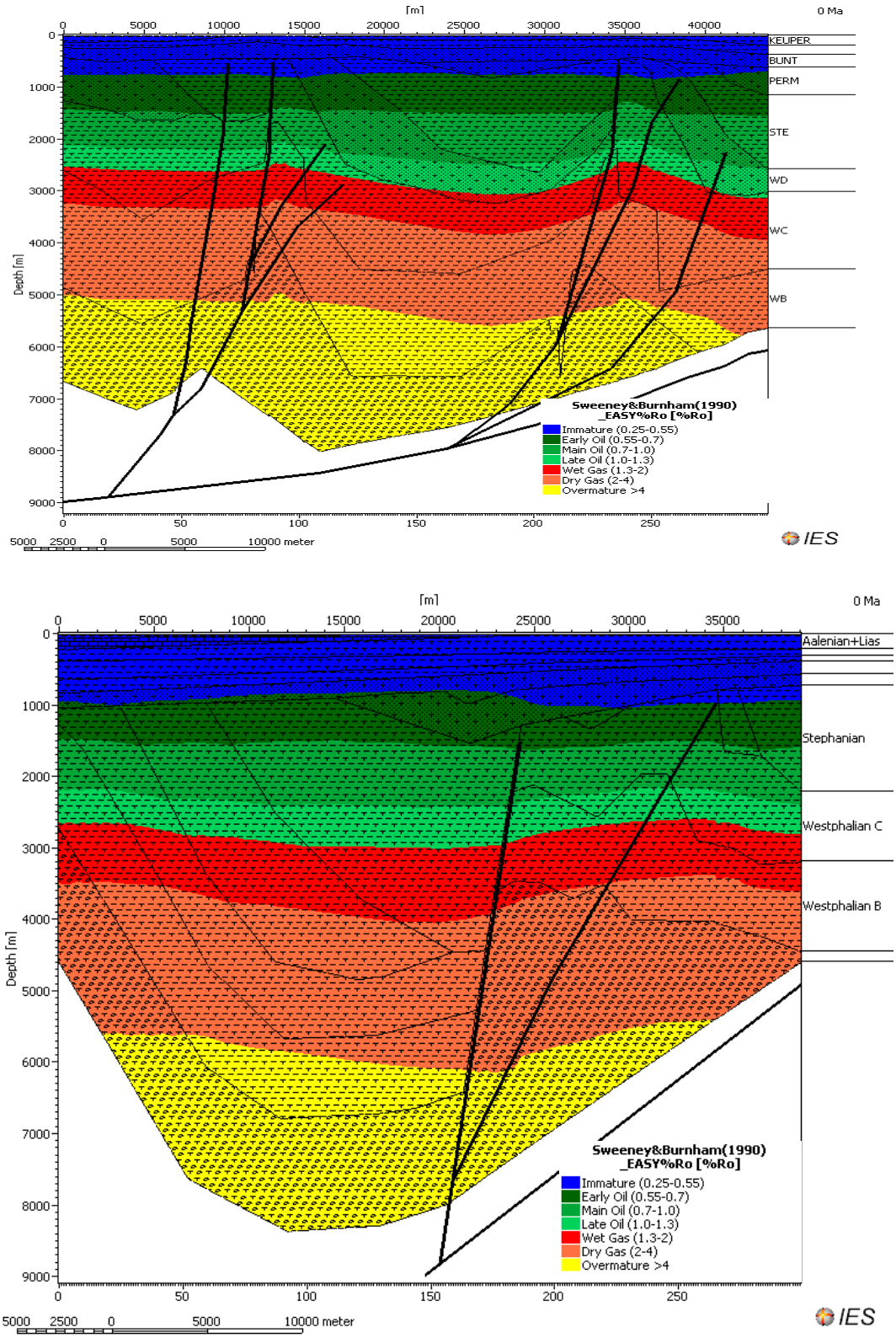

Fig. 13: Hydrocarbon maturity in the EPLY 02-LOR 09 and TOUL 08 seismic lines
Bunt : Buntsandstein, Perm : Permian, Ste : Stephanian and WB, C and D : Westphalian B, C and D.

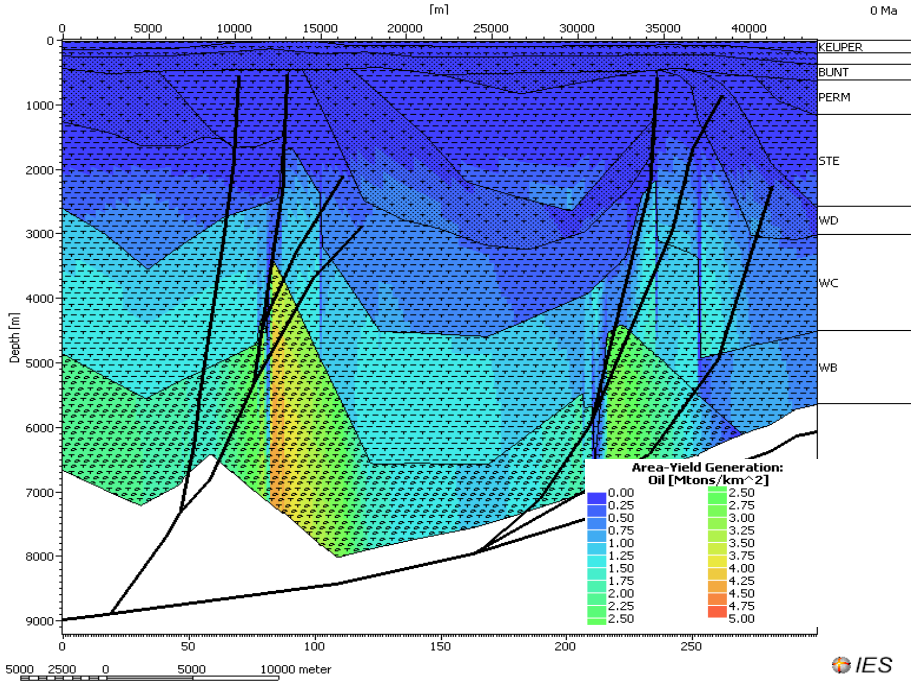

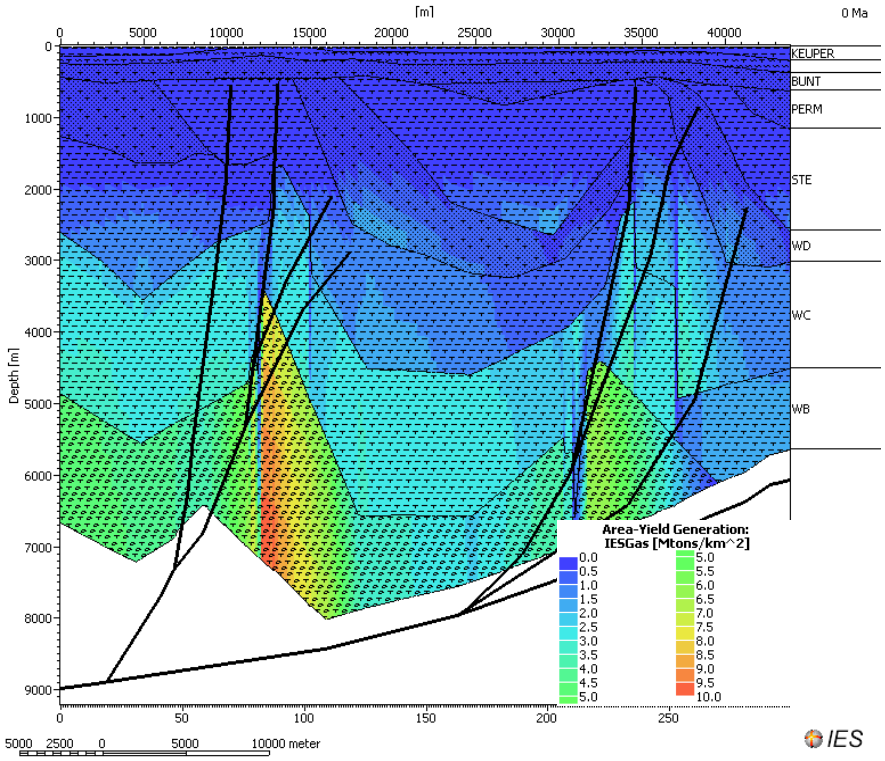

Fig. 14: Oil and gas generation in the EPLY 02-LOR 09 seismic lines
Bunt : Buntsandstein, Perm : Permian, Ste : Stephanian and WB, C and D : Westphalian B, C and D.

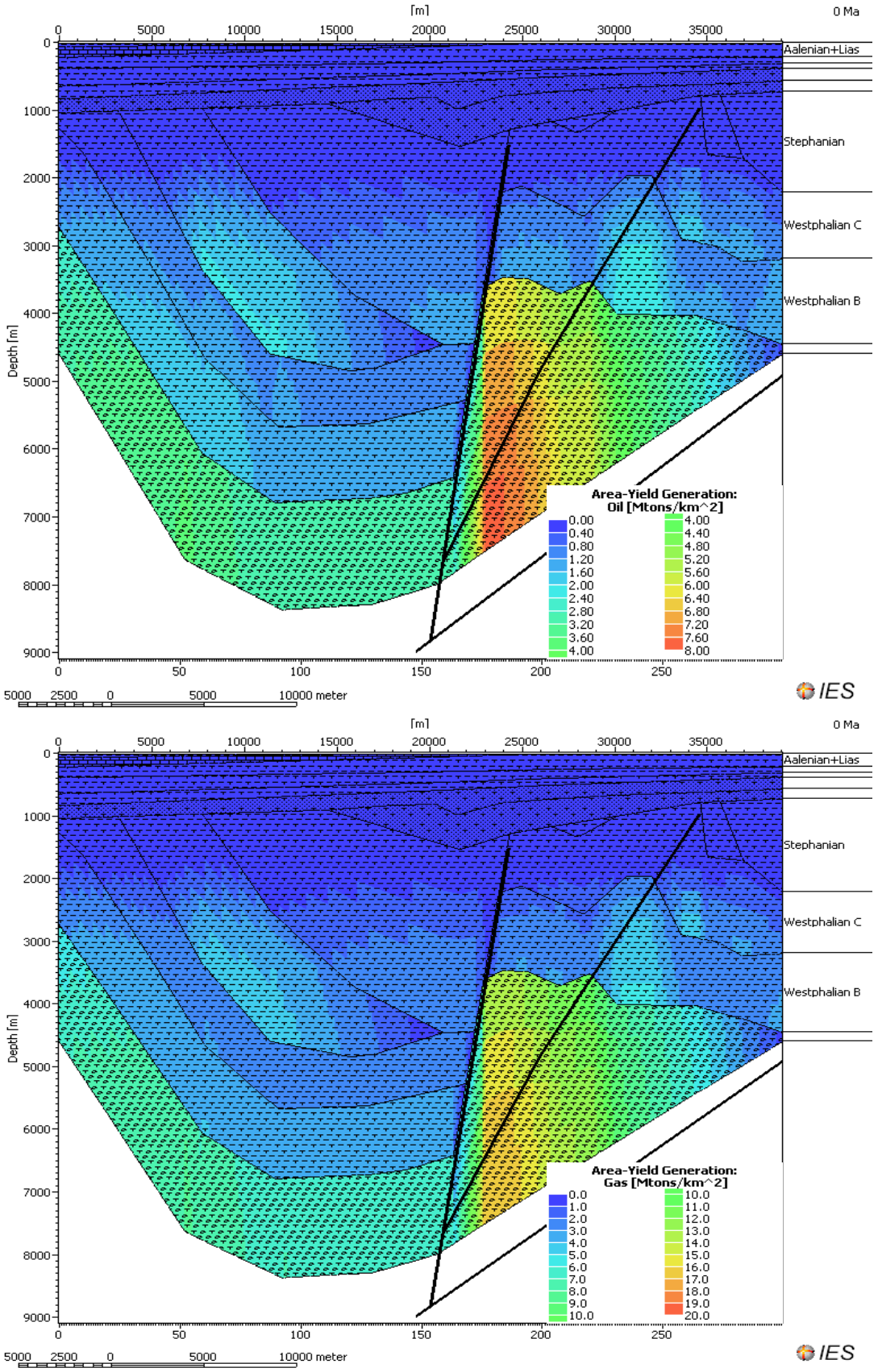

Fig. 15: Oil and gas generation in the TOUL 08 seismic line

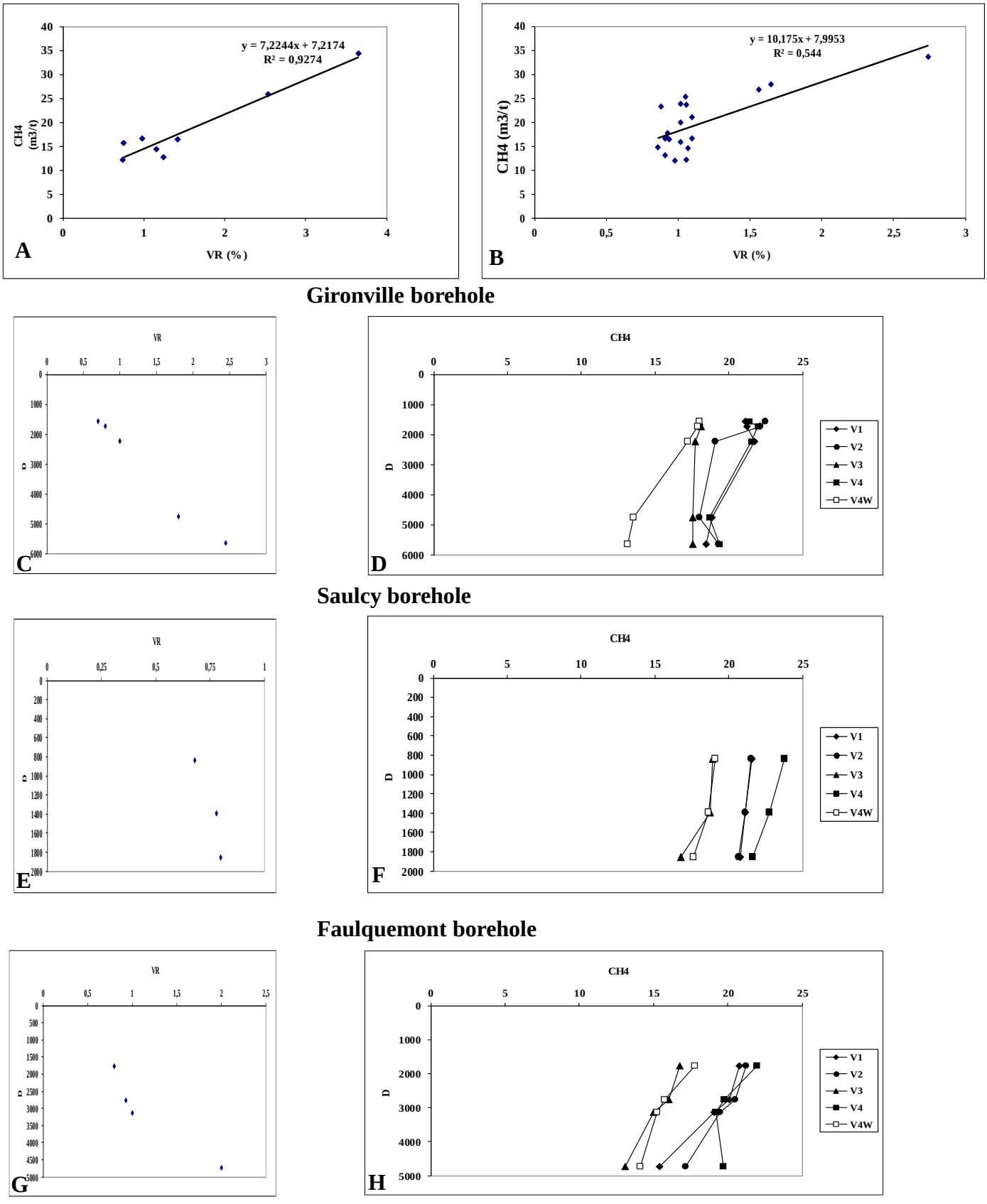

Fig.16: Methane adsorption capacity in coal seams (m^3/ton coal) vs VR (%) after Garnier et al. (2011) in A and Hildenbrand et al. (2006) in B, and VR (%) and methane adsorption capacity (V, m^3/ton coal) vs. depth (m) in Gironville (CD), Saulcy (EF) and Faulquemont (GH) boreholes
V1 at 300 Ma, V2 at 250 Ma, V3 at 140 Ma, V4 at 0 Ma for dry coal and
V4W at 0 Ma for a water content equal to 2.5 %.

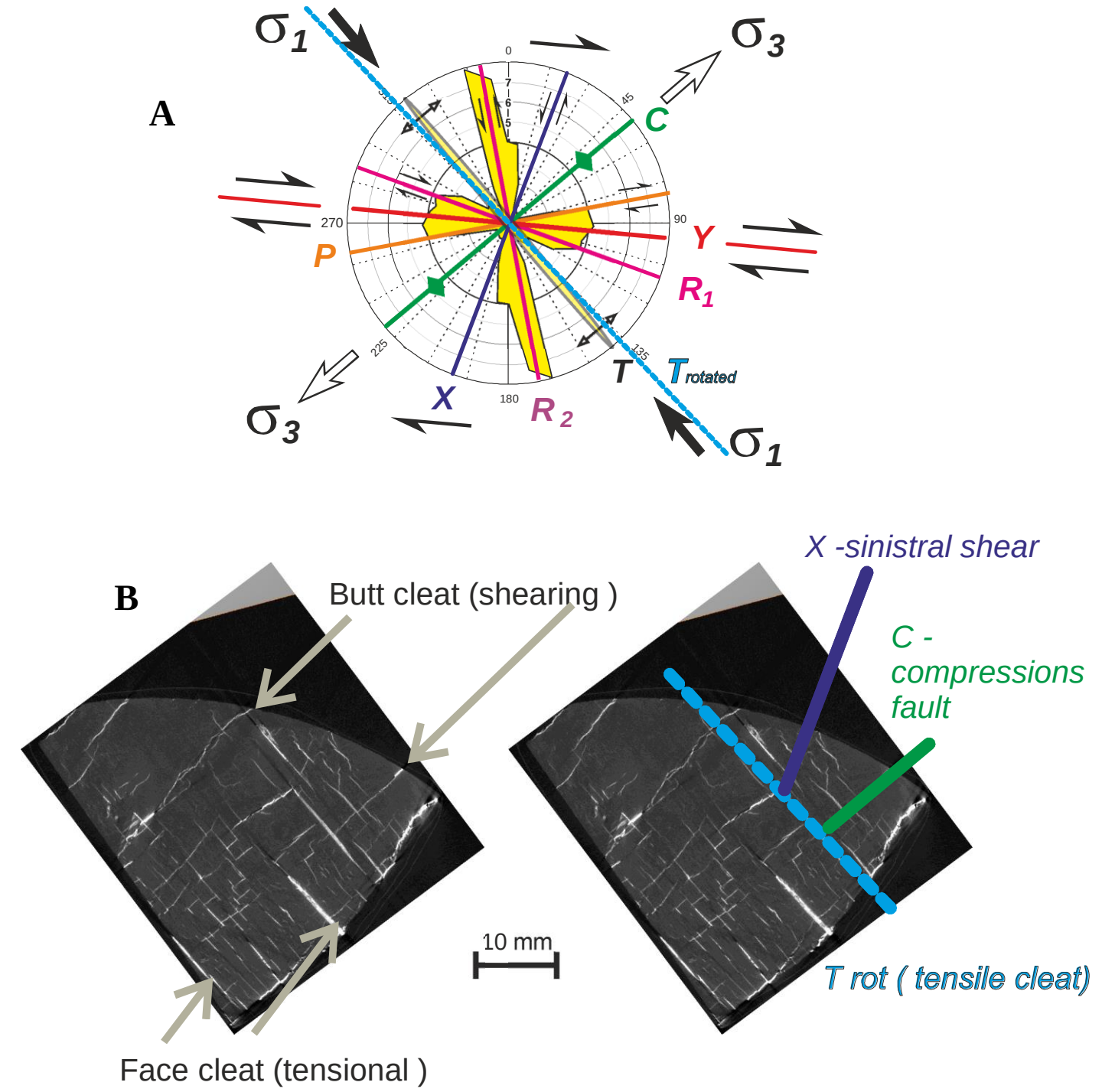

Fig. 17: Application of tomography for analyzing cleat system in a coal sample from coal seam 10 (1239m depth) in Westphalian D of Tritteling 1 borehole

A: Direction of diaclases (in yellow) in the coal seams 6, 8 and 9 after underground mapping in coal mine Faulquemont after Bles and Lozes (1980) ; B: Face and Butt cleats in the coal sample

A

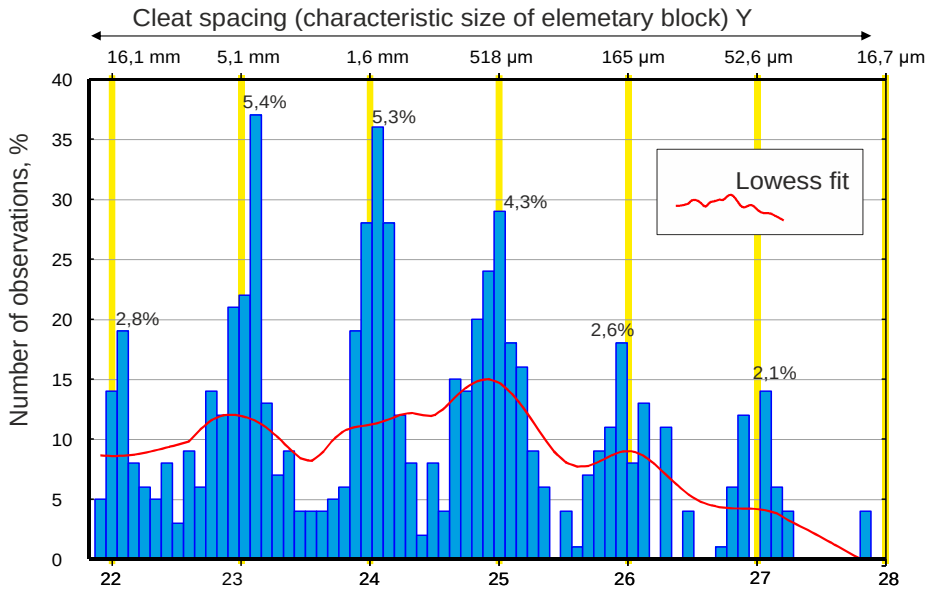

B

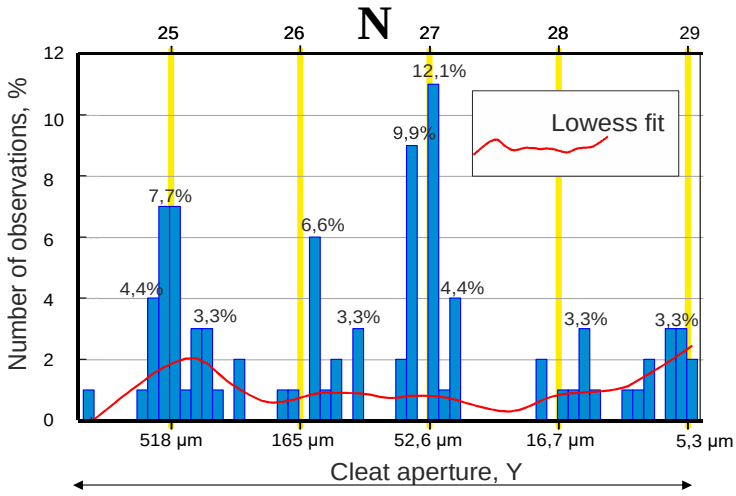

C

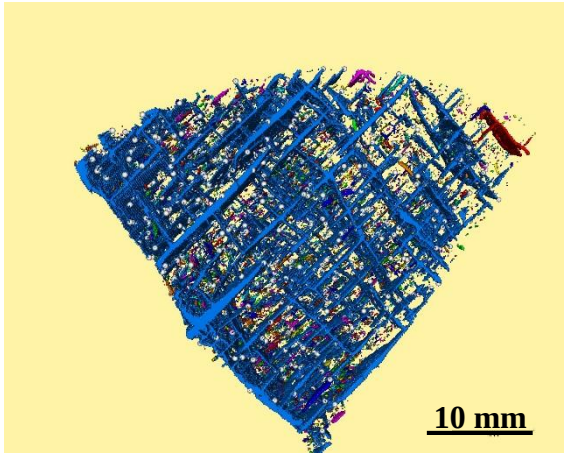

Fig. 18: Application of tomography for analyzing cleat spacing (A), aperture (B) and connectivity (C) in a coal sample from coal seam 10 (1239m depth) in Westphalian D of Tritteling 1 borehole

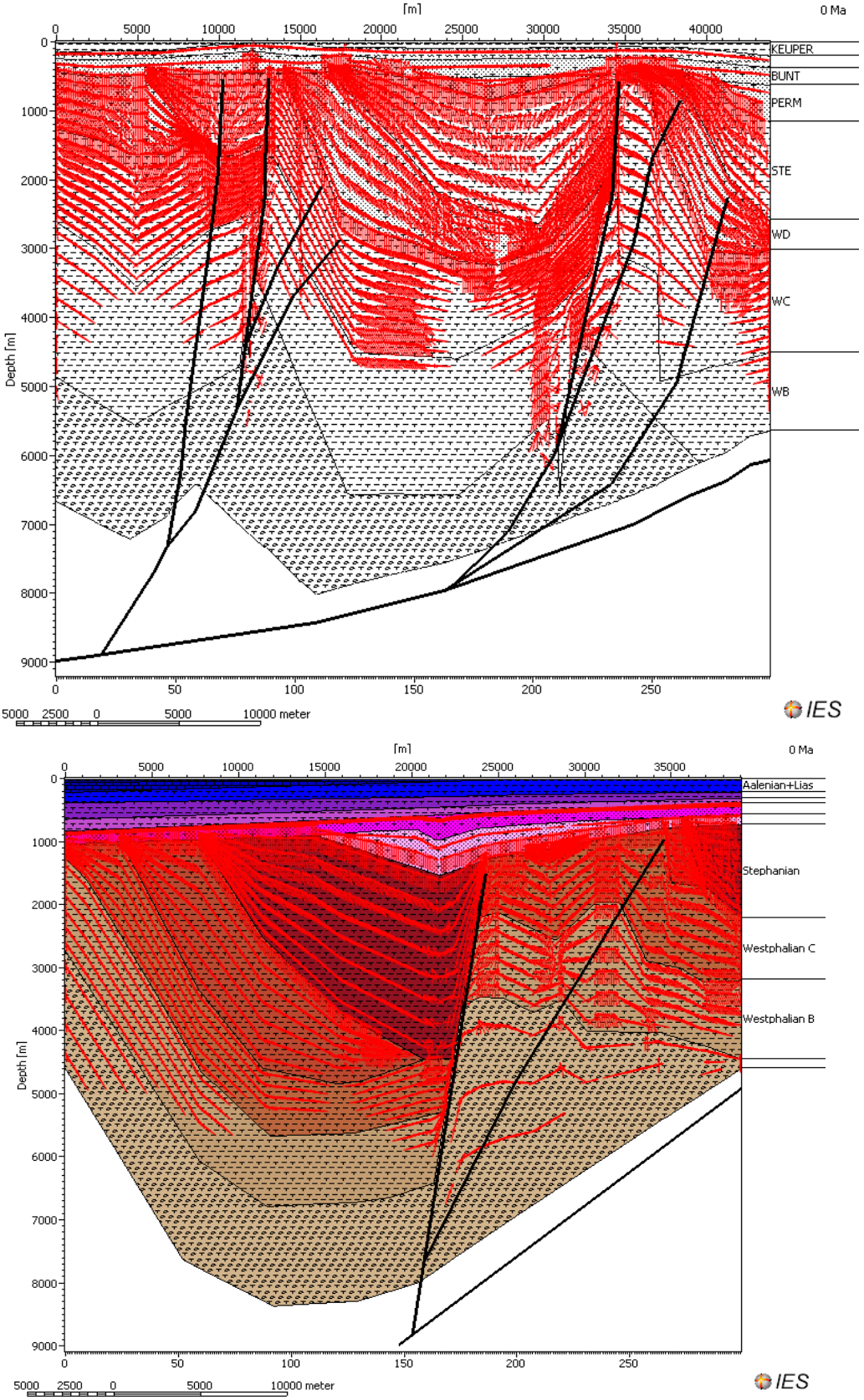

Fig. 19: Gas migration pathways in the EPLY 02-LOR 09 and Toul 08 seismic lines
Bunt : Buntsandstein, Perm : Permian, Ste : Stephanian and WB, C and D : Westphalian B, C and D.

Boreholes	X (km)	Y (km)	Z (m)	Final Depth (m)	Final Formation	Company	Year
Chaumont 001 (CMN 001)	861.178	1137.131	302.65	1890	Westphalian B	DUPONT DE NEMOURS	1995
Chevraumont 1 (CHV 1)	858.952	1094.577	319	2500	Permian rhyolite	ESSO REP	1984
Culey 1 (CEY 1)	814.8	1120.5	244	3705	Westphalian B	ESSO REP	1982
Diebling (DBL 1)	933.919	1659.99	287	1423	Westphalian C	EGL	2007
EST 433	819.170	1098.686	358.28	2001	Buntsandstein	ANDRA	2008
Faulquemont 1 (FQT 1)	910.65	1162.32	299.4	1554	Westphalian D	WINDSOR	1988
Folschviller 1A (FOLS 1A)	918.471	1613.81	264	1306	Westphalian D	EGL	2006
Forcelles 5 (LFO 5)	877.83	1090.75	329	379	Buntsandstein	EURAFREP	1981
Francheville 1 (FRV 1)	863	1123	233	3859	Westphalian B	ESSO REP	1983
Gironville 101 (LGi 101)	844.916	1127.850	244.35	5683	Late Viséan	SNPA	1963
Lerouville 1 (LLR1)	833	1124	246	1546	Westphalian C	SNPA	1962
Merlebach (Reumau mine shaft)	926.2	1171.58	283	922	Westphalian C	HBL	1923
Lorettes 001 (LRT 001)	884.5764	1146.5768	238.05	1847	Westphalian B	DUPONT DE NEMOURS	1995
Morhange 1 (LMo 1)	918.917	1144.177	271.64	2669	Westphalian	SNPA	1954
Pont-à-Mousson (PM 101)	881.74	1143.86	228	2430	Westphalian B	SNPA	1959
Saulcy 001 (SUY 001)	895.844	1157.204	231,2	1999	Westphalian B	DUPONT DE NEMOURS	1995
Tritteling 1 (TRIT1)	912.841	1161.359	364.5	1239	Westphalian D	EGL	2014
Trois-Fontaines 106 (TF 106)	796.283	1114.470	210	1937	Basement	EURAFREP	1987
Velaine-sous-amance 49 (Va 49) for Rn 8	890.99	1118.78	274.55	550	Buntsandstein	GDF	1977
Vaxy 001 (VXY 1)	908	1138	250	2124	Westphalian	LUNDIN	2008

Table 1: Location of boreholes
X and Y coordinates are from Lambert 1 grid reference.

Lithology	Thermal conductivity ($W.m^{-1}.K^{-1}$)	Heat capacity ($kcal.Kg^{-1}.K^{-1}$)	Density ($Kg.m^{-3}$)
Anhydrite	4.81	0.174	2850
Chalk	2.85	0.197	2700
Coal	0.5	0.204	1680
Dolomite	3.81	0.202	2836
Halite	5.69	0.206	2160
Limestone	2.83	0.195	2710
Sandstone	3.12	0.178	2660
Claystone	1.98	0.213	2680

Table 2: Thermal conductivity (at temperature=20°C), heat capacity (at temperature=20°C) and density of pure lithology

GIRONVILLE 101 Name	Top	Base	Present Thickness	Eroded Thickness	Deposition Age from	to	Erosion age from	to	Lithology	VR	TOC	HI	OM Type	P Type	HF
	m	m	m	m	Ma	Ma	Ma	Ma	%	%	%	mg HC g^{-1} TOC			mW m^{-2}
Late Cretaceous	0	0	0	300	99.6	65.5	65.5	50	Ma (14)+Ch (86)						40
Early Cretaceous	0	0	0	22	145.5	99.6	50	45	Gr (8)+Ma (8)+Cl (47)+Sa (37)						42
Tithonian	0	0	0	111	150.8	145.5	45	40	Gr (9)+Mu (87)+Cl (4)						45
Kimmeridgian	0	0	0	147	155.6	150.8	40	35	Mu (45)+Ma (55)						45
Oxfordian	0	0	0	286	159.7	155.6	35	30	Gr (68)+Mu (32)						47
Callovian+Oxfordian	0	75	75	80	164.7	159.7	30	0	Gr (5)+Mu (1)+Ma (40)+Cl (54)		1	50	III	SR	47
Bathonian+Bajocian	75	227	152		171.6	164.7			Gr (51)+Mu (40)+Ma (9)					RE	50
Aalenian+Liassic	227	573	346		199.6	171.6			Mu (6)+Ma (14)+Cl (80)		5	300	II	SR	50
Rhetian+Keuper	573	810	237		228.7	199.6			Cl (51)+Sa (3)+Do (3)+An (7)+Ha (36)					SE	52
Muschelkalk	810	945	135		242.2	228.7			Cl (63)+Sa (12)+Do (25)					RE	55
Buntsandstein	945	1121	176		249.5	242.2			Cl (12)+Sa (82)+Co (6)	0.6				RE	60
Permian	1121	1121	0	400	284.5	270	270	249.5	Sa (100)					RE	60
Stephanian	1121	1450	329	400	305	300	300	284.5	Sa (21)+Cl (73)+Coal (6)		4	100	III	SR	60
Westphalian D	1450	1450	0	400	308	306	306	305	Sa (21)+Cl (73)+Coal (6)		1	150	III	SR	50
Westphalian C	1450	1885	435		311.7	308			Sa (19)+Cl (58)+Coal (23)	0.7-0.8	4	150	III	SR	50
Westphalian B	1885	3470	1585		313	311.7			Sa (26)+Cl (60)+Coal (15)	1-1.8	1	150	III	SR	50
Namurian+Westphalian A	3470	5675	2205		328.3	313			Co (44)+Sa (19)+Cl (36)+Coal (1)	1.9-2.4	1	150	III	SR	50
Basement	5675	7675	2000		400	328.3			Basement						

Table 3: Input data for the Gironville 001 borehole

An: anhydrite, Ch: chalk, Cl: claystone, Co: Conglomerate, Do: dolomite, Gr: limestone (grainstone), Ha: halite, HF: heat flow, HI: hydrogen index, OM: organic matter, Ma: marl, Mu: limestone (mudstone), P: petroleum data, RE: reservoir rock, Sa: sandstone, SE: seal rock, SR: source rock, TOC: total organic carbon, VR: vitrinite reflectance.

Boreholes	Culey		Francheville		Chevraumont		Chaumont 001		Lorettes 001		Saulcy 001		Vaxy		Faulquemont		Rn 8	
Formations	Present Thick	Eroded Thick	Present Thick	Eroded Thick	Present Thick	Eroded Thick	Present Thick	Eroded Thick	Present Thick	Eroded Thick	Present Thick	Eroded Thick	Present Thick	Eroded Thick	Present Thick	Eroded Thick	Present Thick	Eroded Thick
	m	m	m	m	m	m	m	m	m	m	m	m	m	m	m	m	m	m
Late Cretaceous	0	300	0	300	0	300	0	300	0	300	0	100	0	0	0	0	0	100
Early Cretaceous	0	22	0	22	0	22	0	22	0	22	0	20	0	0	0	0	0	20
Tithonian	0	111	0	111	0	111	0	111	0	111	0	111	0	111	0	50	0	111
Kimmeridgian	165		0	147	0	147	0	165	0	165	0	165	0	147	0	50	0	147
Oxfordian	172		0	286	0	286	0	172	0	172	0	172	0	286	0	286	0	286
Callovian+Oxfordian	164		0	155	0	155	0	164	0	164	0	164	0	155	0	155	0	155
Bathonian+Bajocian	213		33	118	156		98	115	0	213	0	213	0	213	0	364	0	210
Aalenian+Liassic	401		400		227		292,5		28	373	0	401	0	401	0	300	20	205
Rhetian+Keuper	319		305		273		232,5		319		0	319	200	119	0	225	290	
Muschelkalk	209		152		135		150		209		161	48	213		150		155	
Buntsandstein	92		261		205		225		92		400		387		625		300	
Permian	0	400	182	200	345		0	200	0	200	0	200	33	200	0	200		
Stephanian	54	400	1249	250	1159		54	250	54	250	0	250	819		1000			
Westphalian D	0	400	473	300			0	300	0	300	0	300	0	300	1350			
Westphalian C	1117		410				803		472,5		1283		473	300	1600			
Westphalian B	1344		1585				1585		1585		1585		1585		600			
Namurian+Westphalian A	750		2205				2205		2207		1585		2200		1000			
Basement	2000		2000		2000		2000		2000		2000		2000		2000			

Table 4: Present and eroded thickness (Thick) of formations in boreholes

Boreholes	Culey 001	Francheville 1	Chevraumont	Chaumont 001	Lorettes 001	Saulcy 001	Vaxy	Faulquemont
Formations	Lithology	Lithology	Lithology	Lithology	Lithology	Lithology	Lithology	Lithology
Permian	Sa (100)	Sa (100)	Rhyolite+Sa (41)+Cl (59)	Sa (100)	Sa (100)	Sa (100)	Sa (100)	Sa (100)
Stephanian	Sa (59)+Cl (35)+Coal (6)	Sa (48)+Cl (49)+Coal (3)	Rhyolite+Sa (25)+Cl (69)+Coal (6)	Sa (29)+Cl (45)+Coal (16)	Co (6)+Sa (30)+Cl (60)+Coal (4)	Co (6)+Sa (30)+Cl (60)+Coal (4)	Sa (43)+Cl (51)+Coal (6)	Co (3)+Sa (64)+Cl (29)+Coal (4)
Westphalian D	Sa (26)+Cl (68)+Coal (5)	Sa (57)+Cl (31)+Coal (12)		Sa (29)+Cl (45)+Coal (16)	Co (36)+Sa (26)+Cl (37)+Coal (1)	Co (36)+Sa (26)+Cl (37)+Coal (1)	Co (36)+Sa (26)+Cl (37)+Coal (1)	Co (47)+Sa (20)+Cl (28)+Coal (5)
Westphalian C	Sa (30)+Cl (60)+Coal (9)	Sa (83)+Cl (11)+Coal (6)		Sa (38)+Cl (56)+Coal (6)	Sa (35)+Cl (58)+Coal (7)	Sa (12)+Cl (70)+Coal (18)	Sa (30)+Cl (50)+Coal (20)	Sa (25)+Cl (70)+Coal (5)
Westphalian B	Sa (46)+Cl (45)+Coal (9)	Sa (42)+Cl (45)+Coal (12)		Sa (17)+Cl (78)+Coal (5)	Sa (33)+Cl (57)+Coal (10)	Sa (12)+Cl (69)+Coal (19)	Co (13)+Sa (43)+Cl (43)+Coal (1)	Co (14)+Sa (69)+Cl (12)+Coal (5)
Namurian+Westphalian A	Co (44)+Sa (19)+Cl (36)+Coal (1)	Co (44)+Sa (19)+Cl (36)+Coal (1)		Co (44)+Sa (19)+Cl (36)+Coal (1)	Co (44)+Sa (19)+Cl (36)+Coal (1)	Co (44)+Sa (19)+Cl (36)+Coal (1)	Co (44)+Sa (19)+Cl (36)+Coal (1)	Co (15)+Sa (69)+Cl (15)+Coal (1)
Basement	Basement	Basement	Basement	Basement	Basement	Basement	Basement	Basement

Table 5: Permian and Carboniferous Facies

Cl: claystone, Co: conglomerate and Sa: sandstone.

Boreholes			Gironville					Culey					Francheville				
Formations	OM Type	P Type	Sample Depth m	VR %	TOC %	HI mg HC g^{-1} TOC	HF mW m^{-2}	Sample Depth m	VR %	TOC %	HI mg HC g^{-1} TOC	HF mW m^{-2}	Sample Depth m	VR %	TOC %	HI mg HC g^{-1} TOC	HF mW m^{-2}
Late Cretaceous							40					40					40
Early Cretaceous							42					42					42
Tithonian							45					45					45
Kimmeridgian							45					45					45
Oxfordian							47					47					47
Callovian+Oxfordian	III	SR			1	50	47			1	50	47					47
Bathonian+Bajocian		RE					50					50					50
Aalenian+Liassic	II	SR			5	300	50			5	300	50					50
Rhetian+Keuper		SE					52					52					52
Muschelkalk		RE					55					55					55
Buntsandstein		RE					60					60					60
Permian		RE					60					60					60
Stephanian	III	SR			4	100	60					60			3	100	60
Stephanian	III	SR			4	100	60			4	100	60	2580	0.94	3	100	60
Westphalian D	III	SR			1	150	50			1	100	50			12	100	50
Westphalian D	III	SR			1	150	50			1	100	50	2851	1.07	12	100	50
Westphalian C	III	SR			4	150 (100-200)	50			4	100	50			6	100	50
Westphalian C	III	SR	1571	0.7	4	150 (100-200)	50	1813	0.8	4	100	50	3110	1.15	6	100	50
Westphalian C	III	SR	1738	0.8	4	150 (100-200)	50	2785	0.9	4	100 (146-65)	50			6	100	50
Westphalian B	III	SR	2240	1	1	150 (100-200)	50	2906	0.9	2	100	50	3610	1.34	12	100	50
Westphalian B	III	SR			1	150 (20-100)	50	3590	1.6	2	100 (65-36)	50	3750	1.42	12	100	50
Namurian+Westphalian A	III	SR	4750	1.8	1	150 (10)	50			1	100	50			1	100	50
Namurian+Westphalian A	III	SR	5640	2.45	1	150 (0)	50			1	100	50			1	100	50
Basement																	

Boreholes	Chevraumont					Chaumont 001					Lorettes 001				
Formations	Sample Depth m	VR %	TOC %	HI mg HC g^{-1} TOC	HF mW m^{-2}	Sample Depth m	VR %	TOC %	HI mg HC g^{-1} TOC	HF mW m^{-2}	Sample Depth m	VR %	TOC %	HI mg HC g^{-1} TOC	HF mW m^{-2}
Late Cretaceous					40					40					40
Early Cretaceous					42					42					42
Tithonian					45					45					45
Kimmeridgian					45					45					45
Oxfordian					47					47					47
Callovian+Oxfordian					47					47					47
Bathonian+Bajocian					50					50					50
Aalenian+Liassic					50					50					50
Rhetian+Keuper					52					52					52
Muschelkalk					55					55					55
Buntsandstein					60					60					60
Permian					400					60					60
Stephanian	1436	1.4	6	100	400			5	100	60			4	150	60
Stephanian	2000	3	6	100	400			5	100	60			4	150	60
Westphalian D								6	100	50			1	150	50
Westphalian D								6	100	50			1	150	50
Westphalian C						1301	0.64	6	100	50	1110	0.71	7	150 (100-200)	50
Westphalian C						1622	0.71	6	100	50	1229	0.75	7	150	50
Westphalian C						1731	0.81	6	100	50	1808	0.78	7	150	50
Westphalian B								5	100	50			10	150	50
Westphalian B								5	100	50			10	150	50
Namurian+Westphalian A								1	100	50			1	150	50
Namurian+Westphalian A								1	100	50			1	150	50
Basement															

Boreholes	Saulcy 001					Vaxy					Faulquemont				
Formations	Sample Depth m	VR %	TOC %	HI mg HC g^{-1} TOC	HF mW m^{-2}	Sample Depth m	VR %	TOC %	HI mg HC g^{-1} TOC	HF mW m^{-2}	Sample Depth m	VR %	TOC %	HI mg HC g^{-1} TOC	HF mW m^{-2}
Late Cretaceous					40					40					40
Early Cretaceous					42					42					42
Tithonian					45					45					45
Kimmeridgian					45					45					45
Oxfordian					47					47					47
Callovian+Oxfordian					47					47					47
Bathonian+Bajocian					50					50					50
Aalenian+Liassic					50					50					50
Rhetian+Keuper					52					52					52
Muschelkalk					55					55					55
Buntsandstein					60					60					60
Permian					60					60					60
Stephanian			4	150	60			6	100	60			4	100	60
Stephanian			4	150	60			6	100	60			4	100	60
Westphalian D			1	150	50			1	100	50	1775	0.8	4	100	50
Westphalian D			1	150	50			1	100	50	2775	0.9	5	100	50
Westphalian C	841	0.68	18	50 (100-20	50			20	100	50	3125	1	5	100	50
Westphalian C	1393	0.78	18	50 (100-27	50	2070	0.7	20	100	50	4725	2	5	100	50
Westphalian C	1853	0.8	18	50 (100-22	50	2105	0.81	20	100	50			5	100	50
Westphalian B			19	150	50			1	100	50			5	100	50
Westphalian B			19	150	50			1	100	50			5	100	50
Namurian+Westphalian A			1	150	50			1	100	50			1	100	50
Namurian+Westphalian A			1	150	50			1	100	50			1	100	50
Basement															

Table 6: OM and petroleum data and Heat Flows

HF: heat flow, HI: hydrogen index, OM: organic matter, P: petroleum data, RE: reservoir rock, SE: seal rock, SR: source rock, TOC: total organic carbon, VR: vitrinite reflectance.

Name	HF(mW/m)	T Erosion (m)	P Erosion (m)	M Erosion (m)	C Erosion (m)	Oil window	Gas window	WA TR(%)	WB TR(%)	WCD+ST TR(%)
Gironville 1	50 (W)-60 (SP)-50 (Tr)-40 (Te-R)	2146	1200	946	320	WCD	WAB	70 to 100	20 to 70	10 to 20
Culey 1	50 (W)-60 (SP)-50 (Tr)-40 (Te-R)	1633	1200	433	320	WCD	WAB	70 to 90	20 to 70	10 to 20
Francheville 1	50 (W)-60 (SP)-50 (Tr)-40 (Te-R)	1889	750	1139	320	WD+ST	WABC	80 to 100	70 to 80	10 to 70
Chevraumont 1	400 (P)-50 (Tr)-40 (Te-R)	1026	0	1026	320		ST			50 to 100
Chaumont 1	50 (W)-60 (SP)-50 (Tr)-40 (Te-R)	1799	750	1049	320	WC	WAB	50 to 90	20 to 50	10 to 20
Lorettes 1	50 (W)-60 (SP)-50 (Tr)-40 (Te-R)	2270	750	1520	320	WC	WAB	70 to 90	10 to 70	5 to 10
Saulcy 1	50 (W)-60 (SP)-50 (Tr)-40 (Te-R)	2665	750	1920	320	WC	WAB	80 to 100	30 to 80	10 to 30
Saulcy 2	50 (W)-60 (SP)-50 (Tr)-40 (Te-R)	2435	750	1700	100	WC	WAB	80 to 100	30 to 80	5 to 30
Lerouville 1	50 (W)-60 (SP)-50 (Tr)-40 (Te-R)	1889	750	1139	320	WBC	WA	70 to 90	40 to 70	20
PAM 1	50 (W)-60 (SP)-50 (Tr)-40 (Te-R)	1889	750	1139	320	WBC	WA	70 to 86	20 to 50	10 to 20
PAM 2	50 (W)-60 (SP)-50 (Tr)-40 (Te-R)	1889	750	1139	320	WBC	WA	70 to 90	20 to 50	10 to 20
Vaxy 1	50 (W)-60 (SP)-50 (Tr)-40 (Te-R)	2554	800	1754	320	ST	WABC	80 to 100	50 to 80	10 to 50
Vaxy 2	50 (W)-60 (SP)-50 (Tr)-40 (Te-R)	2234	800	1434	0	ST	WABC	80 to 100	50 to 80	5 to 50
Faulquemont 1	50 (W)-60 (SP)-50 (Tr)-40 (Te-R)	1630	200	1430	0	ST	WCD	90 to 100	80 to 90	10 to 80
TOUL 08ELB	50 (W)-60 (SP)-50 (Tr)-40 (Te-R)	946	0	946	320	WCD+ST	WABC	90 to 100	90 to 100	30 to 80
Gironville Extr. 1D	50 (W)-60 (SP)-50 (Tr)-40 (Te-R)	946	0	946	320	WCD	WABC	90 to 100	90 to 100	30 to 80
EPLY 07B	50 (W)-60 (SP)-50 (Tr)-40 (Te-R)	1049	0	1049	320	WCD+ST	WAB	90 to 100	60 to 90	10 to 60
Chaumont Extr. 1D	50 (W)-60 (SP)-50 (Tr)-40 (Te-R)	1049	0	1049	320	WC	WAB	90 to 100	60 to 90	10 to 60
EPLY 06E	50 (W)-60 (SP)-50 (Tr)-40 (Te-R)	1520	0	1520	320	ST	WABCD	90 to 100	90 to 100	20 to 80
Lorettes Extr. 1D	50 (W)-60 (SP)-50 (Tr)-40 (Te-R)	1520	0	1520	320		WABC	90 to 100	90 to 100	20 to 80
EPLY 02C	50 (W)-60 (SP)-50 (Tr)-40 (Te-R)	1915	0	1920	320-0	ST	WABCD	90 to 100	90 to 100	20 to 90
Saulcy Extr. 1D	50 (W)-60 (SP)-50 (T)-40 (Te-R)	1600	0	1600	100		WABCD	90 to 100	90 to 100	20 to 90
Vaxy Extr. 1D	50 (W)-60 (SP)-50 (T)-40 (Te-R)	1600	0	1600	0	ST	WABCD	90 to 100	90 to 100	20 to 90

Table 7: Heat flow, Erosion thickness, Oil and gas windows and OM transformation rates (TR)

C: Cretaceous, Extr.: 1D extraction from 2D, M: Mesozoic, P: Paleozoic, ST: Stephanian, T: total, TR: OM transformation rates, Tr: Triassic, Te-R: Tertiary-Recent, W: Westphalian, WA, B, C and D: Westphalian A, B, C and D.

Name	Expulsion Time (Ma)	Oil generation (Mtons/km3)	Gas generation (Mtons/km3)	Oil storage (Mtons/km3)	Gas storage (Mtons/km3)
Gironville 1	311 (Moscovian)-100 (Late Cretaceous)- 0	2 (WAB) <0.2 (WCD)	2 to 5 (WAB) <0.5 (WCD)	<0.035	<0.01
Culey 1	308 (Moscovian)-60 (Early Tertiary)- 0	1 to 2 (WAB) <1 (WC)	2 to 5 (WAB) <2 (WC)	<0.02	<0.01
Francheville 1	312 (Moscovian)-60 (Early Tertiary)- 0	2 to 3.5 (WAB)	5 to 8 (WAB) <3 (WCD) <1 (ST)	<0.12 (WCDST) <0.01 (WAB)	<0.02 (WCDST) <0.002 (WAB)
Chevraumont 1	300 (Permian)-270 (Permian)	1 to 1.2 (ST)	2 to 2.6 (ST)	<0.5 (ST)	<0.03 (ST)
Chaumont 1	311 (Moscovian)-60 (Early Tertiary)- 0	1.5 to 2.6 (WAB) <0.13 (WC)	2 to 5.6 (WAB) <0.28 (WC)	0.02 to 0.2 (WBC) <0.02 (WA)	0.01 (WBC) <0.003 (WA)
Lorettes 1	312 (Moscovian)-60 (Early Tertiary)- 0	1 to 2.6 (WAB) <0.13 (WC)	1 to 5.8 (WAB) <0.29 (WC)	<0.01 (WA) <0.1 (WB) 0.01 WC	.002 (WA) 0.01 (WB) <0.004 (W
Saulcy 1	312 (Moscvian)-140 (Early Cretaceous)- 0	2 to 5.1 (WAB) 0.25 to 2 (WC)	6 to 11 (WAB) 0.6 to 6 (WC)	<0.014 (WA) 0.1 to 0.2 (WBC)	<0.01 (WABC)
Saulcy 2	312 (Moscovian)-100 (Late Cretaceous)- 0	2 to 5 (WAB) 0.2 to 2 (WC)	4 to 10 (WAB) 0.5 to 4 (WC)	<0.028 (WA) 0.1 (WBC)	<0.011 (WABC)
Lerouville 1	312 (Moscovian)-60 (Early Tertiary)- 0	1 to 2.8 (WAB) <0.14 (WC)	3 to 6 (WAB) <0.3 (WC)	0.1 to 0.2 (WB) <0.018 (WA WC)	<0.002 (WAC) 0.02 (WB)
PAM 1	312 (Moscovian)-60 (Early Tertiary)- 0	1 to 2.5 (WAB) <0.13 (WC)	1 to 5 (WAB) <0.28 (WC)	0.1 to 0.15 (WB) <0.02 (WA WC)	<0.002 (WAC) 0.01 (WB)
PAM 2	312 (Moscovian)-60 (Early Tertiary)- 0	2 to 2.6 (WAB) <0.13 (WC)	0.5 to 6 (WAB) <0.29 (WC)	0.1 to 0.15 (WB) <0.02 (WA WC)	<0.003 (WAC) 0.02 (WB)
Vaxy 1	311 (Moscovian)-100 (Late Cretaceous)- 0	<0.22 (WAST) 2 to 4 (WB) 4.5 (WC)	<0.5 (WAST) 4 to 8 (WB) 9.6 (WC)	<0.02 (WAB) <0.12 (WCST)	<0.003 (WAB) <0.01 (WCST)
Vaxy 2	311 (Moscovian)-100 (Late Cretaceous)- 0	1.5 to 3.5 (WAB) 3 (WC) <0.2 (ST)	4 to 8 (WAB) 5 (WC) <0.38 (ST)	<0.014 (WAB) <0.1 (WCST)	<0.002 (WAB) <0.01 (WCST)
Faulquemont 1	300 (Permian)-100 (Late Cretaceous)-0	1 (WD) 2 to 3 (WBC)	3 (WD) 3 to 6 (WBC)	0.1 (WD)	0.01 (WD)
TOUL08ELB	300 (Permian)-100 (Late Cretaceous)-0	1 (WD ST) 2 to 6 (WABC)	1 to 2 (WD ST) 5 to 10 (WABC)	<1 (WST)	<2 (WST)
Gironville Extr. 1D	300 (Permian)-100 (Late Cretaceous)-0	3 to 5 (WA) 1 to 3 (WB) <1 (WCD)	9 to 11 (WA) 3 to 8 (WB) <1 (WCD)	<0.5 (W)	<0.2 (W)
EPLY07B	300 (Permian)-100 (Late Cretaceous)-0	4 to 7 (WA) 1 to 3 (WB) <1 (WCDST)	5 to 20 (WA) 1 to 5 (WB) <1 (WCDST)	<2 (W)	<2.5 (W) higher in WA
Chaumont Extr. 1D	300 (Permian)-100 (Late Cretaceous)-0	4 to 6 (WA) 1 to 2 (WB) <1 (WCD)	10 to 14 (WA) 2 to 3 (WB) <2 (WCD)	<0.3 (WAC) 0.5 (WB)	<0.56 (WBC) 2 (WA)
EPLY06E	300 (Permian)-100 (Late Cretaceous)-0	<1 (WCDST) 2 (WB) 4 to 6 (WA)	<2 (WCDST) 3 to 5 (WB) 10 (WA)	<2 (WST)	<0.5 (WST)
Lorettes Extr. 1D	300 (Permian)-100 (Late Cretaceous)-0	<0.275 (WC) 1 to 2 (WB) 4 to 5 (WA)	<0.6 (WC) 1 to 4 (WB) 9 to 12 (WA)	<1 (W)	<0.3 (W)
EPLY02C	300 (Permian)-100 (Late Cretaceous)-0	1 (WBCDST) 2 to 3 (WA)	0.5 to 2 (WBCDST) 5 to 10 (WA)	<20 (WST)	<4 (WST)
Saulcy Extr. 1D	300 (Permian)-100 (Late Cretaceous)-0	<1 (WBC) 2 to 3 (WA)	<2 (WBC) 4 to 6 (WA)	<0.5 (W)	1 to 15 (WA) <1 WBC
Vaxy Extr. 1D	300 (Permian)-100 (Late Cretaceous)-0	<1 (WBCDST) 1.7 (WA)	<1 (WBCD) 3.75 in WA 0.2 to 3 (ST)	<0.2 (WST)	<0.8 (WST)

Table 8: Expulsion time, and oil and gas generation and storage

Extr.: 1D extraction from 2D, ST: Stephanian, WA, B, C and D: Westphalian A, B, C and D.

Borehole	VR (%)	D (m)	V1 (m3/ton coal)	V2 (m3/ton coal)	V3 (m3/ton coal)	V4 (m3/ton coal)	V4W (m3/ton coal)
Gironville	0,7	1571	21,15	22,5	18	21,4	18
	0,8	1738	21,25	22,15	18,1	22	17,88
	1	2240	21,77	19,07	17,72	21,5	17,25
	1,8	4750	18,89	18	17,54	18,7	13,55
	2,45	5640	18,44	19,34	17,54	19,4	13,13
Saulcy	0,68	841	21,6	21,6	18,9	23,8	19,1
	0,78	1393	21,15	21,15	18,73	22,79	18,62
	0,8	1853	20,8	20,8	16,75	21,65	17,62
Faulquemont	0,8	1775	20,8	21,25	16,75	21,96	17,79
	0,93	2775	20,1	20,5	16,03	19,79	15,75
	1	3125	19,1	19,5	15,02	19,18	15,24
	2	4725	15,4	17,16	13,11	19,7	14,09

Table 9: Adsorption capacity of coal (m3/ton coal) in Gironville, Saulcy and Faulquemont boreholes V1 at 300 Ma, V2 at 250 Ma, V3 at 140 Ma, V4 at 0 Ma for dry coal and V4W at 0 Ma for a water content equal to 2.5 %.